Pei Xianjun (Orcid ID: 0000-0001-5282-0607)

An analytically formulated structural strain method for fatigue evaluation of welded components incorporating nonlinear hardening effects

Xianjun Pei[1] and Pingsha Dong[2]

Abstract

An analytically formulated structural strain method is presented for performing fatigue evaluation of welded components by incorporating nonlinear material hardening effects by means of a modified Ramberg-Osgood power-law hardening model. The modified Ramberg-Osgood model enables a consistent partitioning of elastic and plastic strain increments during both loading and unloading. For supporting two major forms of welded structures in practice, the new method is applied for computing structural strain defined with respect to a through-thickness section in plate structures and cross-section in piping systems. In both cases, the structural strain is formulated as the linearly deformation gradient on their respective cross-sections, consistent with the "plane sections remain plane" assumption in structural mechanics. The structural strain based fatigue parameter is proposed and has been shown effective in correlating some well-known low-cycle and high-cycle fatigue test data, ranging from gusset-to-plate welded plate connections to pipe girth welds.

Key wards: Low cycle fatigue, structural strain method, modified Ramberg-Osgood model, mesh-insensitive method, stress concentration

[1] Ph.D. student, Department of Naval Architecture and Marine Engineering, University of Michigan, Ann Arbor, MI, 48109, xpei@umich.edu

[2] Corresponding author, Professor, Department of Naval Architecture and Marine Engineering, University of Michigan, Ann Arbor, MI, 48109, dongp@umich.edu

1. Introduction

Fatigue evaluation of welded components has always been challenging due to the presence of various forms of geometric discontinuities such as sharp notches at weld locations, which introduce stress and/or strain singularity, leading to mesh-size sensitivity in finite element (FE) calculations and strain gauge size/location sensitivity in experimental measurements [1]. Historically, there are several approaches for mitigating some of these issues in stress determination. These include nominal stress approach [2,3], surface-extrapolation based hot-spot stress approach [4,5], equivalent notch radius based local stress or strain approach [6,7], and more recently, mesh-insensitive traction structural stress method which is also referred to as master S-N curve method [8].

Nominal stress approach, also referred to as weld classification method [2] or weld category method [9], limits its applications to simple components subjected to simple loading conditions, on which strength of materials theory can be reasonably applied for nominal stress determination. In addition, a proper selection of an applicable S-N curve out of many requires judgment call. The surface-extrapolation approach assumes that weld toe stress can be represented by a hot spot stress definition obtained using an extrapolated stress to a weld location (e.g., at weld toe) from specified surface positions, e.g., at 0.4t and 1t (t: plate thickness) from weld toe position. Such a hot spot stress definition seems not immune to mesh-size sensitivity [e.g., 1,8], in addition to its lack of a well-argued mechanics basis. A similar argument can be made regarding equivalent notch stress method by assuming a radius, such as using 0.05mm for thin-walled welded structures [10,11] and 1mm for typical steel and aluminum weldments [12,13].

As for the mesh-insensitive traction structural stress method, it was formulated by imposing equilibrium conditions through a novel use of nodal forces and moments available from FE output [1] and shown to provide a consistent stress concentration characterization for differentiating effects of different joint types and loading conditions [1,8] on fatigue behaviors. Its relevance to fracture mechanics based traction stress definition enabled the development of master S-N curve by collapsing a large amount of fatigue test data obtained from various joint geometries, loading modes, and plate

thicknesses into a narrow band [8,14], which has been adopted by ASME Section VIII Division 2 Code since 2007 [8]. The method has been shown capable of correlating multiaxial test data [15] as well as some low cycle fatigue test data [16] in piping components. Regarding the latter, Dong et al [16] analyzed a series of low cycle fatigue tests of girth welded pipes including some well-known tests performed by Markl [17] and more recently by Scavuzzo et al [18] under displacement-controlled conditions (see Fig. 1). Dong and Yang [19] investigated a large amount of girth-welded umbilical tubes subjected to large deformation reeling/unreeling conditions. Both studies have showed that the low cycle fatigue test data analyzed falls onto the same master S-N curve scatter band as high cycle fatigue data if a pseudo elastic nominal load (F_a) or nominal stress is available from a load-displacement plot, as illustrated in Fig. 1c.

The pseudo elastic load method shown in Figs. 1b-1c dates back to Markl's work [17] which has since been used as a basis for low cycle fatigue design in ASME Codes and Standards [20]. Consider either cantilever beam bending or 4-point beam bending cyclic fatigue tests, a cyclic loading was accomplished by imposing a constant displacement amplitude (δ_a). The corresponding actual load amplitude the component experienced should be F_m, measured from a load cell reading. For low cycle fatigue analysis, where the structure beyond yield limit, a pseudo-elastic load F_a was obtained by extrapolating the linear portion of the stabilized load-displacement curve up to the specified applied displacement amplitude (δ_a) (see Fig. 1c). The pseudo-elastic nominal stress is then calculated by a simple elastic beam bending formula under the pseudo-elastic load:

$$\sigma = \frac{M_a}{I} R \qquad M_a = F_a L \tag{1}$$

Here R and I are outer radius and moment of inertia of the pipe, respectively, while M_a is the moment corresponding to the pseudo-elastic load. As shown in [16] and also demonstrated in Fig. 1d, as long as such a load-displacement curve is available, the pseudo-elastic stress representation of low cycle fatigue data provides a demonstrated transferability between low cycle and high cycle fatigue regime, as shown in Fig. 1d. One major limitation is that it cannot be used for

low cycle fatigue evaluation under load-controlled conditions without a relevant load-displacement curve. The other is that for more complex structural components other than pipes, there exists no characteristic load-displacement curve, e.g., a flat head vessel under high amplitude of cyclic pressure loading conditions.

The pseudo-elastic stress calculation procedure given in Eq.(1) implies that the assumption that "a plane of beam section remains as a plane during deformation" continues to be valid at weld location in elastic-plastic deformation regime, at least for fatigue characterization purpose. Equivalently, it suggests that the linear deformation gradient across the whole pipe section that can be used to correlate fatigue test data, rather than relying on localized notch strains induced by weld geometric discontinuities, which are, to a large extent, already contained in the test data when test components represent typical weld quality and weld bead geometric characteristics. The use of linear strain gradient across a pipe section or a plate through-thickness section is consistent with the traction based structural stress definition within linear elastic deformation context, which is determined in terms of through-thickness membrane and bending parts at any given weld location by imposing equilibrium conditions in both through-thickness and along weld line [1,8]. It is this connection that has led to the recent developments of structural strain method (see [21-23]) for extending the existing traction structural stress method to applications in low cycle fatigue regime with some degree of success, e.g., under the assumption of elastic perfectly plastic material without considering any strain hardening effects. Along this line, the treatment of low cycle fatigue for welded plate components is given in Dong et al [21] and for pipe components in Pei et al [22]. Note that in [21], a series of low cycle fatigue tests of plate joints were analyzed by using a structural strain procedure that approximately takes into account of strain hardening effects due to gross-section yielding conditions encountered in fatigue testing.

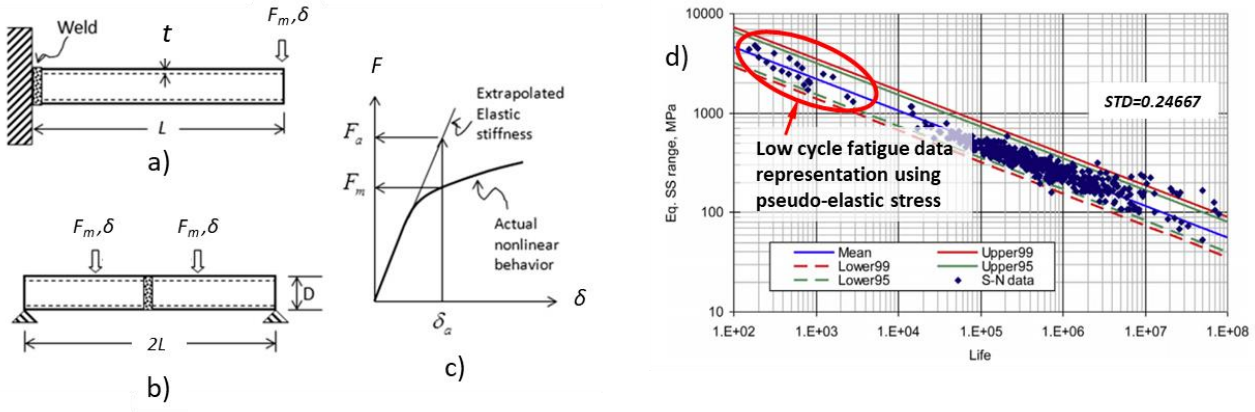

Fig. 1. Original pseudo-elastic stress concept by Markl for analyzing fatigue test data of pipe sections: a) cantilever bending; b) four-point bending; c) pseudo-elastic stress determination using extrapolated pseudo-elastic load using measured load-displacement curve; d) fatigue data analysis results using pseudo-elastic structural stress.

The purpose of this paper is to present a generalized structural strain method that is applicable for fatigue evaluation of both welded plate structures and pipe components by incorporating a more general Ramberg-Osgood strain hardening law so that load-controlled conditions can be effectively treated. The reason for making a distinction between plate and pipe components is that "plane-remaining-plane" conditions is imposed with respect to plate thickness in plate components while the same condition is imposed with respect to the entire pipe section in pipe components. The latter is to be consistent to how fatigue tests have been performed and fatigue failure criteria have been defined historically for piping systems within ASME community [24]. In addition, piping system stress analysis is typically done with beam element models [20] which is consistent with the structural strain definition across a pipe section.

The paper is organized as follows. After introducing the definition of structural strain, analytical formulations governing structural strain development are presented for plate and pipe sections subjected to remote membrane and bending stresses in Sec. 2. In addition, a modified Ramberg-Osgood power law hardening model is presented for facilitating a consistent elastic and plastic strain partitioning which is required for calculating elastic core size that can be directly related to the cross-section plane as a result of elastic-plastic deformation. A robust numerical procedure is then presented for solving

the analytically formulated governing equations in Sec. 3, along with a series of calculation examples for validating the structural strain results obtained from the analytically formulation and by direct finite element computations. Then, low cycle fatigue test data from both welded plate and pipe components are analyzed using the structural strain method developed for demonstrating its effectiveness. Finally, relative contributions to structural strain developments as a result of plane-strain conditions and material hardening effects are discussed in Sec. 5, particularly on how the structural strain calculation procedures may be further simplified if power-law hardening parameters may be not available for fatigue evaluation of welded components in practice.

2. Structural strain definition and formulation

2.1. Structural strain definition

Consider a fillet welded plate structure with a representative cross-section shown in Fig. 2a. Without losing generality, a weld toe fatigue cracking into plate thickness, i.e., along Plane A-A, is considered as shown. Although local stress along the hypothetical crack plane can be highly nonlinear, the corresponding traction structural stress component (i.e., opening stress component with respect crack plane A-A) can be calculated in a mesh-insensitive manner [1,8] in terms of normal membrane part (σ_m) and normal bending part (σ_b) under specified remote loading conditions. Then, an equivalent 2D plate section problem can be described as shown in Fig. 2b, subjected to the same statically equivalent membrane (σ_m) and bending stress (σ_b) that can be expressed as force *N* and moment *M* per unit length. The resulting linear strain distribution (linear deformation gradient) in terms of membrane strain ε_m and bending strain ε_b is defined as structural strain, after imposing both equilibrium conditions and material yield criteria. Similarly, the structural strain with respect to pipe cross section at weld toe position in Fig. 1c acting on plane B-B can be described as shown in Fig. 2d. This structural strain definition is consistent with the traction structural stress definition by suppressing strain singularity at weld toe or weld root.

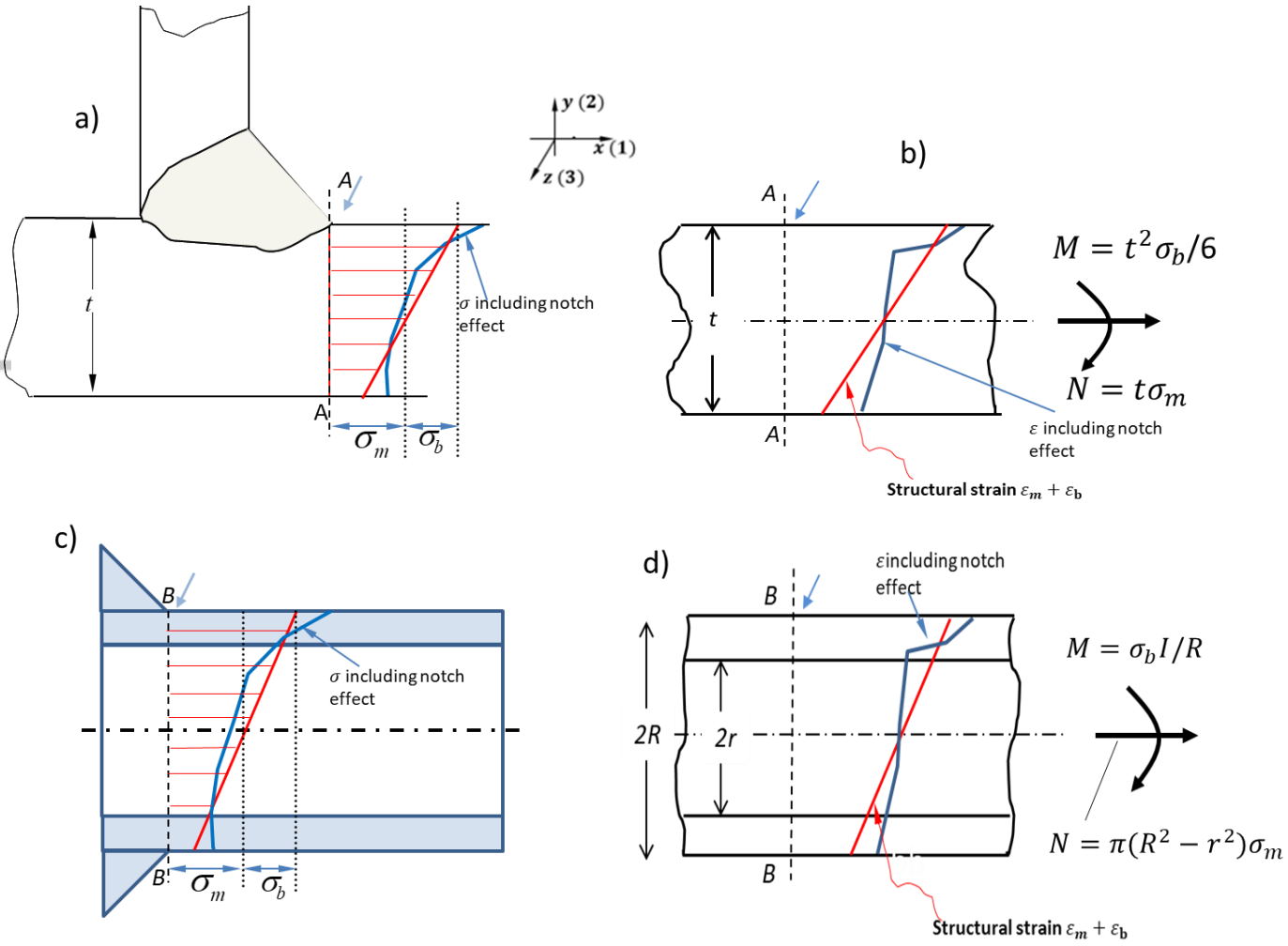

Fig. 2 Structural strain definitions: a) Traction structural stress (σ_m, σ_b) determined on a plate cross-section A-A using mesh-insensitive method [1,8]; b) structural strain ($\varepsilon_m + \varepsilon_b$) at along plate section A-A; c) Traction structural stress (σ_m, σ_b) on pipe cross-section B-B obtained from finite beam element analysis ; d) structural strain ($\varepsilon_m + \varepsilon_b$) at along pipe section B-B

The structural strain in terms of $\varepsilon_m, \varepsilon_b$ shown in Figs. 2b and 2d can be written as a linear deformation gradient described as:

$$\varepsilon_s(y) = \varepsilon_m + \varepsilon_b = ky + b \tag{2}$$

Under general loading conditions, as shown in [1], three traction structural stress components are available and can be extracted in a mesh-insensitive manner on a given hypothetical crack plane, e.g., A-A in Fig. 2a or B-B in Fig. 2c. These are normal traction structural stress (σ_m,σ_b) contributing to Mode I loading and two shear traction structural stresses (τ_m^{II}, τ_b^{II} and $\tau_m^{III}, \tau_b^{III}$) contributing to Modes II and III loading, respectively. The corresponding structural strain definitions can be expressed as:

$$\begin{aligned} \varepsilon_m^{I,II,III} &= \frac{\varepsilon_{\max}^{I,II,III} + \varepsilon_{\min}^{I,II,III}}{2} \\ \varepsilon_b^{I,II,III} &= \frac{\varepsilon_{\max}^{I,II,III} - \varepsilon_{\min}^{I,II,III}}{2} \\ \varepsilon_s^{I,II,III} &= \varepsilon_m^{I,II,III} + \varepsilon_b^{I,II,III} \end{aligned} \tag{3}$$

Here $\varepsilon^{I,II,III}$ corresponds to structural strain components on a hypothetical crack plane subjected to Modes I, II, and III loading conditions. Without losing generality, hereafter it is assumed that only the normal structural strain component (ε^I) is dominant. (Other two components can be treated in exactly the same manner.) A simplified notation can then be used, e.g., using ε_m for representing ε_m^I, ε_b for ε_b^I, and ε_s for ε_s^I.

2.2. Formulation

2.2.1. Material hardening behavior

In two related studies, Dong et al. [21] and Pei et al. [22] adopted elastic perfectly plastic material model in determining structural strains at weld locations in plate and pipe components, such that solutions can be expressed in a closed form in terms of elastically calculated traction structural stresses. Their results indicate an improvement in test data correlation. However, once plastic deformation becomes severe or elastic core size becomes small, elastic perfectly plastic material model can significantly over-estimate structural strain without considering strain-hardening effects, particularly when membrane stress σ_m becomes dominant. To overcome this issue and introduce a more general treatment of material

hardening behaviors, a modified Ramberg-Osgood constitutive relation is presented here, which allows a clear partitioning of elastic and plastic strain increments while maintaining the same power law structure as its original form.

The original Ramberg-Osgood relation was first proposed by Ramberg and Osgood [25], which provides a rather versatile representation of material stress-strain relations for numerous metals and is widely adopted by engineering community [26-28]. The relation describes nonlinear material behavior in terms of total strain:

$$\varepsilon = \frac{\sigma}{E} + \alpha \frac{\sigma_0}{E}\left(\frac{\sigma}{\sigma_0}\right)^m \tag{4}$$

in which ε is the total strain, E is Young's modulus α, m and σ_0 are material parameters obtained in a power law fit of true stress strain curve. Two major deficiencies exist in the original Ramberg-Osgood relation given in Eq. (4): 1) the power term in the equation implies that material exhibits nonlinear deformation behavior even when applied stress σ is well below material nominal yield strength, often referred to as nonlinear elasticity material model; 2) the equation form does not allow a clear separation of elastic and plastic deformations. As a result, linear-elastic unloading behavior and plastic strain accumulation cannot be consistently modeled when dealing with cyclic fatigue loading conditions when incremental plasticity theory is invoked. The former is a prerequisite for determining component cross-section elastic core size.

To overcome the above two deficiencies, a modified Ramberg-Osgood equation is proposed as follows:

$$\varepsilon = \begin{cases} \varepsilon^e = \dfrac{\sigma}{E} \ \ (\sigma \le \sigma_{prop}) \\ \varepsilon^e + \varepsilon^p = \dfrac{\sigma}{E} + \alpha \dfrac{\sigma_0}{E}\left[\left(\dfrac{\sigma}{\sigma_0}\right)^m - r^m\right] \ \ (\sigma > \sigma_{prop}) \end{cases} \tag{5}$$

Here σ_{prop} is the proportional limit of the material and r is defined as

$$r = \frac{\sigma_{prop}}{\sigma_0} \tag{6}$$

which is the ratio of material proportional limit σ_{prop} over reference stress σ_0. The detail explanation of Eq.(5) is given in Appendix A. The modified Ramber-Osgood equation given in Eq.(5) enables a clear separation of material elastic strain from plastic strain, and provides a convenient form for expressing strain hardening effect in terms of plastic strain, i.e.:

$$\sigma = \sigma_0 \left(\frac{E\varepsilon^p}{\alpha\sigma_0} + r^m \right)^{1/m} \tag{7}$$

In dealing with multiaxial stress state, ε^p in Eq.(7) can be replaced by $\bar{\varepsilon}^p$ which is the equivalent plastic strain given by

$$\bar{\varepsilon}^p = \left(\frac{2}{3} \boldsymbol{\varepsilon}^{\mathbf{p}} : \boldsymbol{\varepsilon}^{\mathbf{p}} \right)^{1/2} \tag{8}$$

in which $\boldsymbol{\varepsilon}^{\mathbf{p}}$ is the plastic strain tensor.

To demonstrate the effectiveness of Eq. (5) in representing experimental stress-strain test data, e.g., stainless steel 304, Fig. 3 compares the fitting results between the original Ramberg-Osgood equation (Eq.(4)) and the modified Ramberger-Osgood equation (Eq. (5)) with experimental data. There is no noticeable difference in the fitting results shown in Fig. 3. The introduction of a proportional limit in the form of Eq. (5) allows the partitioning of total strain in terms of elastic and plastic strain components, which enables the determination of structural strain according to the definitions given in Sec. 2.1.

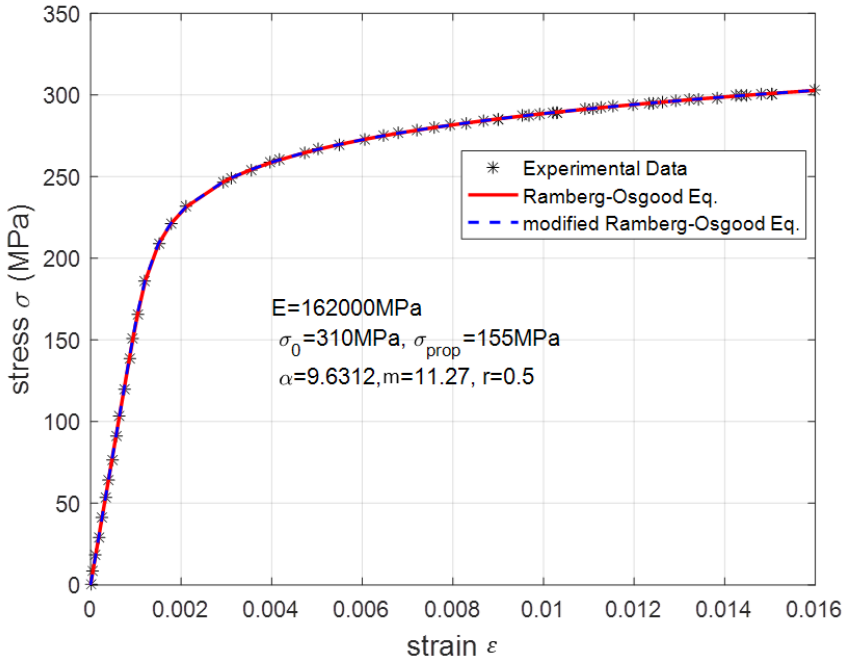

Fig. 3 Comparison of the original Ramberg-Osgood and the modified Ramberg-Osgood fits for representing Stainless Steel 304 stress-strain data

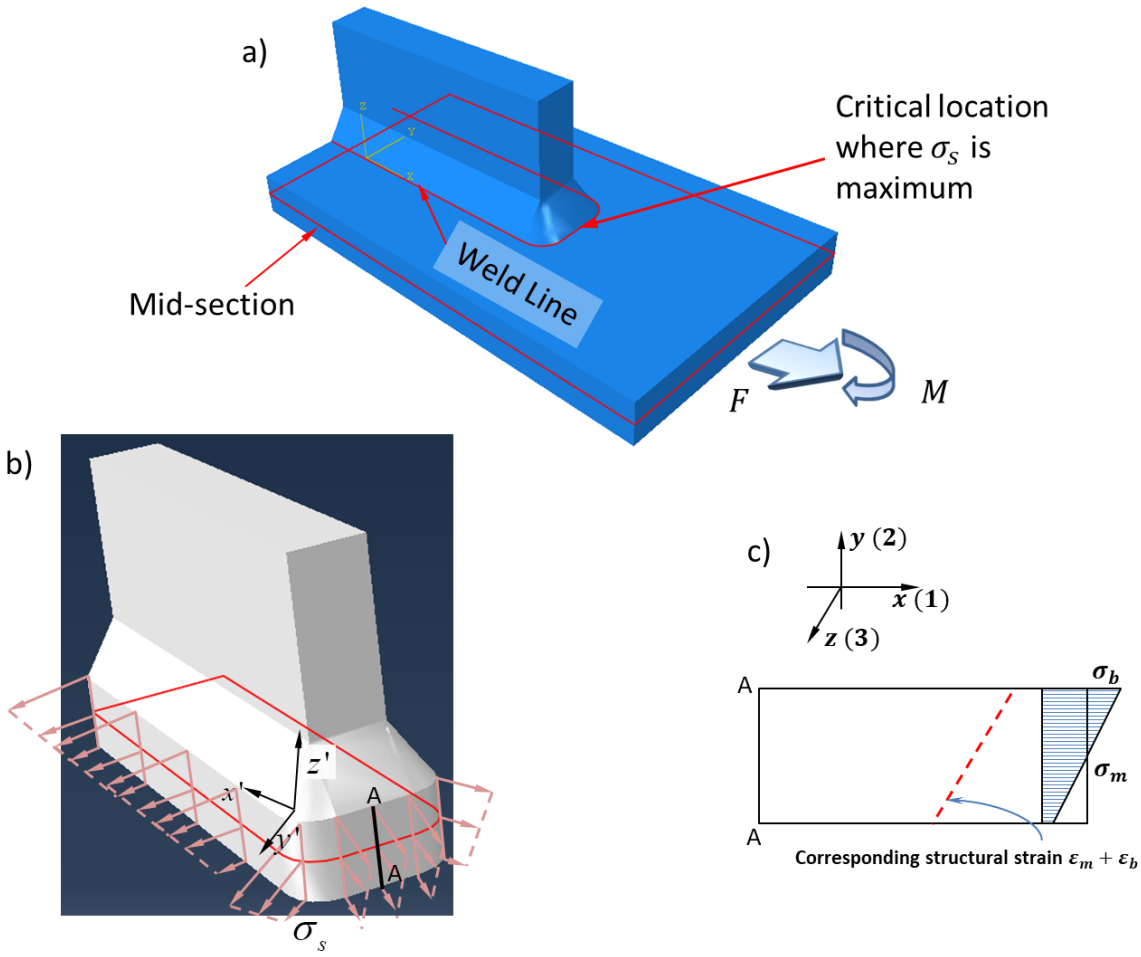

Fig. 4 Traction structural stress determination using mesh-insensitive method given in [1,8]: a) welded plate component under remote loading; b) illustration of traction stress distribution on curvilinear cut at weld toe line into plate thickness; c) structural strain at critical through-thickness section A-A corresponding to traction structural stress (σ_m, σ_b)

2.2.2. Plate section

Consider a welded plate component shown in Fig. 4, in which the highest stress concentration location is as shown when the component is loaded in remote tension or bending on the base plate. By performing the traction structural stress analysis using method provided in [1,8], the structural stress σ_s can be calculated on the curvilinear cut along the entire weld line into base plate thickness (Fig. 4b) in a mesh-insensitive manner. Here $\sigma_s = \sigma_m + \sigma_b$ is the summation of

membrane and bending stress component. With respect to the through-thickness section at the critical location, a 2D cross-section representation under plane strain conditions is shown in Fig. 4c, for which σ_m and σ_b serve as statically equivalent remote load. The corresponding structural strain should satisfy equilibrium conditions, and material constitutive relation represented by the modified Ramberg-Osgood relation described in the proceeding section. Then, the equilibrium equations are:

$$\begin{aligned} \int_{-t/2}^{t/2} \sigma_1(y)dy &= \sigma_m t \\ \int_{-t/2}^{t/2} \sigma_1(y)ydy &= \int_{-t/2}^{t/2} \left(\frac{2\sigma_b}{t} y \right) ydy = \frac{\sigma_b t^2}{6} \end{aligned} \tag{9}$$

Here $\sigma_1(y)$ is the normal stress in x direction, i.e. axis 1 direction. The deformation gradient across plate thickness must be linear to be consistent with the structural strain definitions in Sec. 2.1 and can be written as:

$$\varepsilon_1^{total}(y) = \varepsilon_1^e(y) + \varepsilon_1^p(y) = ky + b \tag{10}$$

where ε_1^{total} is the total structural strain which can be decomposed into plastic strain ε_1^p and elastic strain ε_1^e. The total structural strain is assumed linearly distributed through thickness, which is a generalization of Qian's theory [29].

Elastic stress-strain relationship can be written in 3D Hooke's law form as:

$$\begin{aligned} \boldsymbol{\sigma} &= 2G\boldsymbol{\varepsilon^e} + \lambda Tr\left(\boldsymbol{\varepsilon^e}\right)\boldsymbol{I} \\ \boldsymbol{\varepsilon^e} &= \boldsymbol{\varepsilon}^{total} - \boldsymbol{\varepsilon}^p \end{aligned} \tag{11}$$

where $\boldsymbol{\sigma}, \boldsymbol{\varepsilon}$ are stress and strain tensors, respectively, $\boldsymbol{I}$ is rank-2 isotropic tensor, $Tr(\boldsymbol{\varepsilon^e})$ is the trace of elastic strain tensor, and G is material shear modulus and

$$\lambda = \frac{E\nu}{(1+\nu)(1-2\nu)} \tag{12}$$

which is termed as Lamé parameter.

When a structure undergoes plastic deformation, yield condition must be satisfied in addition to equilibrium and linear deformation gradient conditions, which can be expressed as, in the form of the modified Ramberg-Osgood relationship, assuming isotropic hardening and von Mises yield criterion:

$$f(\sigma_e, \bar{\varepsilon}^p) = \sigma_e - \sigma_0 \left(\frac{E\bar{\varepsilon}^p}{\alpha\sigma_0} + r^m \right)^{1/m} \tag{13}$$

in which σ_e is the von-Mises stress and $\bar{\varepsilon}^p$ is effective plastic strain given in Eq.(8). f represents yield criterion [30]. It should be noticed that based on the Kuhn-Tucker complementarity condition in classical computational plasticity procedure, the yield function is not allowed to be greater than 0 [30], i.e.

$$f(\sigma_e, \bar{\varepsilon}^p) \leq 0 \tag{14}$$

Associative flow rule is used here, which means the direction of the plastic strain increment is defined by $\partial f / \partial \boldsymbol{\sigma}$, i.e.

$$d\boldsymbol{\varepsilon}^{\boldsymbol{p}} = d\gamma \frac{\partial f}{\partial \boldsymbol{\sigma}} \tag{15}$$

In Eq. (15), γ is the plastic multiplier and $\gamma \geq 0$ by definition, and

$$d\boldsymbol{\varepsilon}^{\boldsymbol{p}} = d\gamma \frac{\partial f}{\partial \boldsymbol{\sigma}} = \frac{3}{2} d\gamma \frac{\boldsymbol{\sigma}'}{\sigma_e} \tag{16}$$

when von-Mises yield criterion is used. In Eq. (16), $\boldsymbol{\sigma}'$ is the deviatoric stress tensor.

It is important to point out here the structural strain distribution is fully determined by k and b in Eq.(10). One of the main objectives of this work is to provide an efficient means to solve (k, b) satisfying Eq.(9)-(15), which will be elaborated in Sec. 3.

2.2.3. Pipe section

Piping systems are often analyzed using beam element models for extracting pipe section forces and moments at a girth-welded location, which can be treated as remote loads, as shown in Fig. 5. Without loss of generality, the structure strain analysis procedure for a pipe section in Fig. 5a is illustrated in Fig. 5b. The remote loads in Fig. 5a can be related to pipe cross-section membrane and bending stresses as:

$$\begin{aligned} \sigma_m &= \frac{F}{A} = \frac{F}{\pi\left(R^2 - r^2\right)} \\ \sigma_b &= \frac{MR}{I} = \frac{MR}{\pi\left(R^4 - r^4\right)/4} \end{aligned} \tag{17}$$

The corresponding equilibrium conditions can be expressed as

$$\begin{aligned} \int_{-R}^{R} \sigma_1(x, y) l(y)\, dy &= F = \sigma_m \pi\left(R^2 - r^2\right) \\ \int_{-R}^{R} \sigma_1(x, y) l(y)\, y dy &= M = \frac{\sigma_b I}{R} = \frac{\sigma_b}{R} \times \frac{\pi}{4}\left(R^4 - r^4\right) \end{aligned} \tag{18}$$

Here $l(y)$ is the cord length perpendicular to y axis (Fig.5c). The linear deformation gradient condition must hold here by definition, as given in Eq.(10). It should be noted that linear deformation gradient is not only valid maintained across pipe wall thickness but also across the entire pipe section, as depicted in Fig. 5b in the form of structural strain distribution.

If assuming that the normal stress acting on a beam cross-section in Fig. 5c is the only dominant stress component, the following relations exist based on classical beam theory:

$$\sigma_1 = E\varepsilon_1^e$$
$$\varepsilon_1^{total} = \varepsilon_1^e + \varepsilon_1^p = ky + b \tag{19}$$

The corresponding yield criteria and flow rule can then be simplified as:

$$f(\sigma_e, \bar{\varepsilon}^p) = |\sigma_1| - \sigma_0 \left(\frac{E\bar{\varepsilon}^p}{\alpha\sigma_0} + r^m \right)^{1/m} \tag{20}$$

$$d\bar{\varepsilon}_1^p = d\gamma \times sign(\sigma_1) \tag{21}$$

respectively.

Finally, *k* and *b* in Eq. (19) can be solved by satisfying Eqs. (17) through (21) in order to obtain the structural strain at a weld location in a piping system.

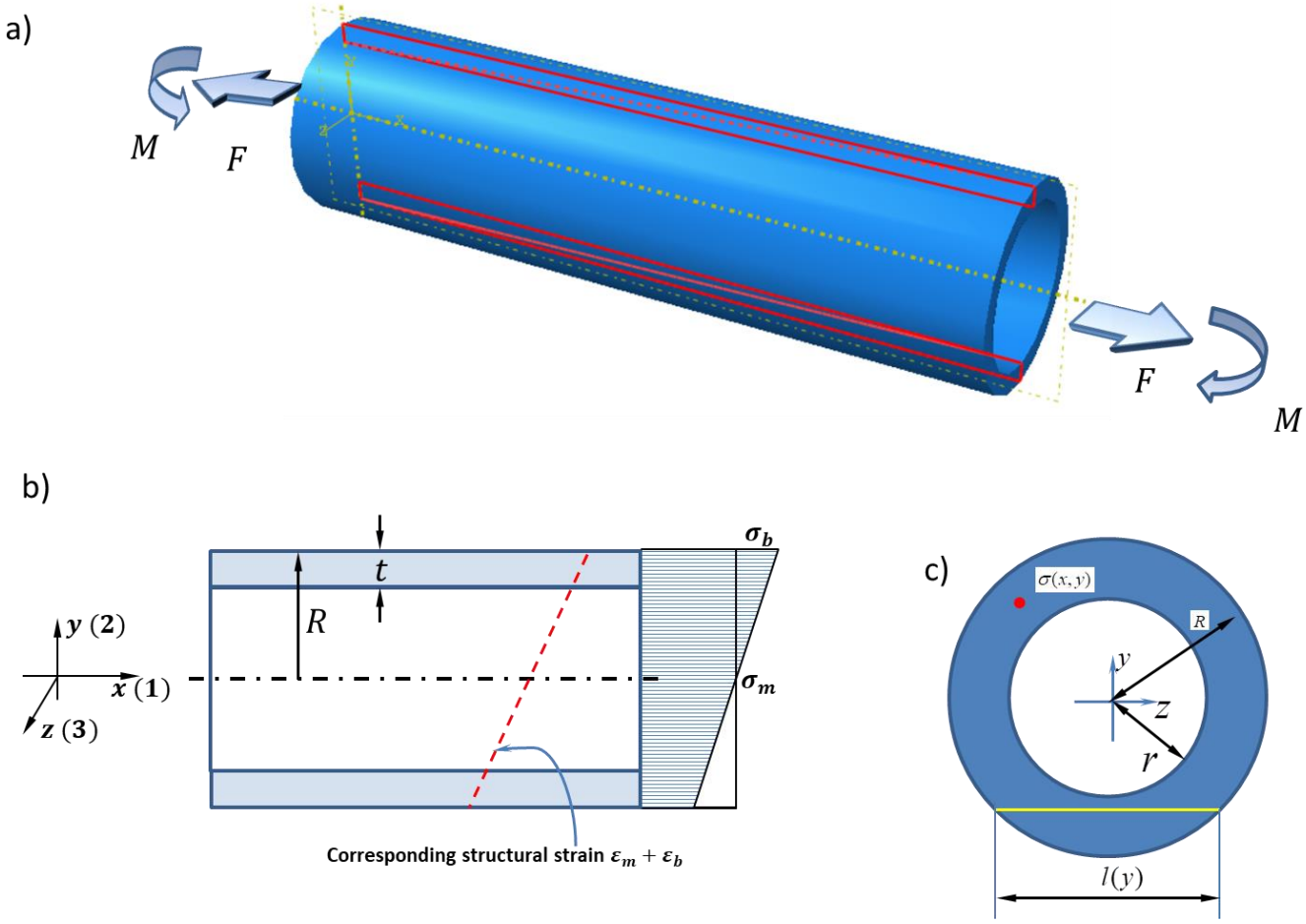

Fig. 5 Traction structural stress determination for a pipe section in welded pipe component: a) Pipe under remote loading; b) longitudinal cross-section of pipe section; c) transverse cross-section

3. Solutions, validations, and Applications

3.1. Numerical solution procedures

The analytical formulations developed for computing structural strain for a plate section (see Sec. 2.2.2) and for pipe section (see Sec. 2.2.3) cannot be solved in closed forms. Numerical method must be used here. In the ensuing sections, a robust numerical procedure will be presented for computing structural strains for both plate and pipe sections.

3.1.1. Plate section

As shown in Fig. 4, the 2D problem illustrated in Fig. 4c can be treated as a plane strain problem, i.e., $\varepsilon_3 = \varepsilon_3^e + \varepsilon_3^p = 0$. It is further assumed that the shear stress and stress normal to plate surface are negligible, i.e. $\tau_{12} \approx 0, \sigma_2 \approx 0$. Then, Eqs. (11)-(12) can be written as:

$$\begin{aligned}\sigma_1 &= \frac{E\varepsilon_1}{\left(1-\nu^2\right)} - \left[\frac{E\varepsilon_1^p}{\left(1-\nu^2\right)} + \frac{\nu E\varepsilon_3^p}{\left(1-\nu^2\right)}\right] \\ \sigma_3 &= \frac{\nu E\varepsilon_1}{\left(1-\nu^2\right)} - \left[\frac{\nu E\varepsilon_1^p}{\left(1-\nu^2\right)} + \frac{E\varepsilon_3^p}{\left(1-\nu^2\right)}\right]\end{aligned} \tag{22}$$

and von-Mises effective stress becomes:

$$\sigma_e = \sqrt{\sigma_1^{\,2} + \sigma_3^{\,2} - \sigma_1\sigma_3} \tag{23}$$

By substituting Eq. (22) into Eq. (9), k and b in Eq. (10) can be related to total strain components and traction stresses by:

$$\begin{aligned}Eb &= \left(1-\nu^2\right)\sigma_m + \int_{-1/2}^{1/2} E\varepsilon_1^p\left(y'\right)dy' + \nu\int_{-1/2}^{1/2} E\varepsilon_3^p\left(y'\right)dy' \\ Ekt &= 2\left(1-\nu^2\right)\sigma_b + 12\int_{-1/2}^{1/2} E\varepsilon_1^p\left(y'\right)y'dy' + 12\nu\int_{-1/2}^{1/2} E\varepsilon_3^p\left(y'\right)y'dy'\end{aligned} \tag{24}$$

in which $y' = y/t$ is the coordinate normalized by plate thickness t.

In view of von-Mises yield criterion and the associative flow rule adopted, the incremental equivalent plastic strain $d\bar{\varepsilon}^p$ and plastic multiplier γ can be related by

$$d\bar{\varepsilon}^{\,p} = \left(\frac{2}{3}d\boldsymbol{\varepsilon}^{\boldsymbol{p}} : d\boldsymbol{\varepsilon}^{\boldsymbol{p}}\right)^{1/2} = \left(\frac{2}{3}\frac{3}{2}d\gamma\frac{\boldsymbol{\sigma}'}{\sigma_e} : \frac{3}{2}d\gamma\frac{\boldsymbol{\sigma}'}{\sigma_e}\right)^{1/2} = d\gamma \tag{25}$$

Finally, when material is under plastic deformation, ($d\bar{\varepsilon}^p > 0$), $d\bar{\epsilon}^p$ can be solved by following the consistency condition in classical plastic theory:

$$f\left(\sigma_e + d\sigma_e, \bar{\varepsilon}^p + d\bar{\varepsilon}^p\right) = 0 \tag{26}$$

To solve Eqs. (22)-(26), an algorithm based on a classical return mapping is implemented for calculating structural strain under traction stress σ_m, σ_b, as shown in Box 1. At beginning of each iteration, the analysis begins with an "elastic step", that is, all plastic strains are set to be equal to the values corresponding to the previous step. Parameters k and b are then solved based on equilibrium conditions described in Eq. (24). Up to Step 1 in Box 1, the equilibrium conditions are met, while the Kuhn-Tucker complementarity may not be. To check the Kuhn-Tucker condition, a trial stress is calculated (note: $(\blacksquare)^{tr}$ is the trial state of ($\blacksquare$)) in Step 2. In Step 3, the trial stress is tested. If Kuhn-Tucker condition is satisfied, the trial state becomes the solution of the problem. Otherwise, the classical return mapping algorithm as shown in Box 2 should be applied to obtain the plastic strain increment.

Box 1: Overall algorithm to obtain structural strain for plate section under plane strain conditions

Set $\varepsilon_{1,(0)}^{p}\left(y_t\right)=0, \varepsilon_{3,(0)}^{p}\left(y_t\right)=0, \bar{\varepsilon}_{(0)}^{p}\left(y_t\right)=0$

while $\left(\left|k_{(i+1)}-k_{(i)}\right|>tol \text{ or } \left|b_{(i+1)}-b_{(i)}\right|>tol \text{ or } \max\left(f_{(i+1)}^{tr}\right)>0\right)$

1. perform "elastic step"

$$\varepsilon_1^{p,tr}\left(y'\right)=\varepsilon_{1,(i)}^{p}\left(y'\right), \varepsilon_3^{p,tr}\left(y'\right)=\varepsilon_3^{p}\left(y'\right), \bar{\varepsilon}^{p,tr}\left(y'\right)=\bar{\varepsilon}^{p}\left(y'\right)$$

$$Eb_{(i+1)}=\left(1-\nu^2\right)\sigma_m+\int_{-1/2}^{1/2}E\varepsilon_1^{p,tr}\left(y'\right)dy'+\nu\int_{-1/2}^{1/2}E\varepsilon_3^{p,tr}\left(y'\right)dy'$$

$$Ek_{(i+1)}t=2\left(1-\nu^2\right)\sigma_b+12\int_{-1/2}^{1/2}E\varepsilon_1^{p,tr}\left(y'\right)y'dy'+12\nu\int_{-1/2}^{1/2}E\varepsilon_3^{p,tr}\left(y'\right)y'dy'$$

$$E\varepsilon_{1,(i+1)}\left(y'\right)=Ek_{(i+1)}ty'+Eb_{(i+1)}$$

2. calculate trial stress

$$\sigma_1^{tr}\left(y'\right)=\frac{E\varepsilon_{1,(i+1)}\left(y'\right)}{1-\nu^2}-\left[\frac{E\varepsilon_1^{p,tr}\left(y'\right)}{1-\nu^2}+\frac{\nu E\varepsilon_3^{p,tr}\left(y'\right)}{\left(1-\nu^2\right)}\right]$$

$$\sigma_3^{tr}\left(y'\right)=\frac{\nu E\varepsilon_{1,(i+1)}\left(y'\right)}{1-\nu^2}-\left[\frac{\nu E\varepsilon_1^{p,tr}\left(y'\right)}{1-\nu^2}+\frac{E\varepsilon_3^{p,tr}\left(y'\right)}{1-\nu^2}\right]$$

$$\sigma_e^{tr}\left(y'\right)=\sqrt{\left(\sigma_1^{tr}\right)^2+\left(\sigma_3^{tr}\right)^2-\sigma_1^{tr}\sigma_3^{tr}}$$

3. check yield criteria and Kuhn-Tucker complementarity condition

$$f^{tr}(\sigma_e^{tr},\bar{\varepsilon}^{p})=\sigma_e^{tr}-\sigma_0\left(\frac{E\bar{\varepsilon}^{p,tr}}{\alpha\sigma_0}+r^m\right)^{1/m}$$

if $f^{tr}\le 0$

Elastic step: set $\left(\bullet\right)_{(i+1)}=\left(\bullet\right)^{tr}$

Else

Plastic step: Proceed with return mapping algorithm (see Box 2)

End if

End while

Box 2: Return mapping algorithm for 2D plane strain problems referred to in Box 1

1.solve $\Delta\bar{\varepsilon}^p$:

$$f(\sigma_e,\bar{\varepsilon}^p)=\sigma_e-\sigma_0\left(\frac{E\bar{\varepsilon}^p}{\alpha\sigma_0}+r^m\right)^{1/m}=0\Rightarrow$$

$$f(\sigma_e,\bar{\varepsilon}^p)=\sigma_e^{tr}-3G\Delta\bar{\varepsilon}^p-\sigma_0\left(\frac{E\bar{\varepsilon}^p}{\alpha\sigma_0}+r^m\right)^{1/m}=0\Rightarrow$$

$$f(\sigma_e,\bar{\varepsilon}^p)=\sigma_e^{tr}-3G\Delta\bar{\varepsilon}^p-\sigma_0\left[\frac{E(\bar{\varepsilon}_t^p+\Delta\bar{\varepsilon}^p)}{\alpha\sigma_0}+r^m\right]^{1/m}=0$$

$$f(\sigma_e,\bar{\varepsilon}^p)=\sigma_e^{tr}-3G\Delta\bar{\varepsilon}^p-\sigma_0\left[\frac{E(\bar{\varepsilon}^{p,tr}+\Delta\bar{\varepsilon}^p)}{\alpha\sigma_0}+r^m\right]^{1/m}=0$$

$$f(\sigma_e,\bar{\varepsilon}^p)=\sigma_e^{tr}-\frac{3E\Delta\bar{\varepsilon}^p}{2(1+\nu)}-\sigma_0\left[\frac{E(\bar{\varepsilon}^{p,tr}+\Delta\bar{\varepsilon}^p)}{\alpha\sigma_0}+r^m\right]^{1/m}=0$$

solve $\Delta\bar{\varepsilon}^p$ (Newton iteration)

2.update strain and stress

$$\Delta\varepsilon_1^p=\frac{3\Delta\bar{\varepsilon}^p}{2\sigma_e^{tr}}\left(\frac{2}{3}\sigma_1^{tr}-\frac{1}{3}\sigma_3^{tr}\right)$$

$$\Delta\varepsilon_3^p=\frac{3\Delta\bar{\varepsilon}^p}{2\sigma_e^{tr}}\left(\frac{2}{3}\sigma_3^{tr}-\frac{1}{3}\sigma_1^{tr}\right)$$

$$\varepsilon_{1,(i+1)}^{p,t+\Delta t}=\varepsilon_{1,(i)}^p+\Delta\varepsilon_1^p$$

$$\varepsilon_{3,(i+1)}^{p,t+\Delta t}=\varepsilon_{3,(i)}^p+\Delta\varepsilon_3^p$$

$$\bar{\varepsilon}_{(i+1)}^p=\bar{\varepsilon}_{(i+1)}^p+\Delta\bar{\varepsilon}^p$$

$$\sigma_{1,(i+1)}=\frac{E}{\left(1-\nu^2\right)}\varepsilon_{1,(i+1)}-\left[\frac{E}{\left(1-\nu^2\right)}\varepsilon_{1,(i+1)}^p+\frac{\nu E}{\left(1-\nu^2\right)}\varepsilon_{3,(i+1)}^p\right]$$

$$\sigma_{3,(i+1)}=\frac{\nu E\varepsilon_{1,(i+1)}}{1-\nu^2}-\left[\frac{\nu E\varepsilon_{1,(i+1)}^p}{1-\nu^2}+\frac{E\varepsilon_{3,(i+1)}^p}{1-\nu^2}\right]$$

Box 2. provides a detailed implementation of classical return mapping algorithm for 2D plane strain problems with material hardening behaviors modeled by the modified Ramberg-Osgood stress-strain relation. During Step 1 of Box 2, effective plastic strain increment $\bar{\epsilon}^p$ is solved by enforcing the consistency condition given in Eq. (26) in which

$$\sigma_e = \sigma_e^{tr} - 3G\Delta\bar{\varepsilon}^p \tag{27}$$

Note that the proof of Eq. (27) is provided in Appendix A. After updating the plastic strain increment, Kuhn-Tucker condition is satisfied while the equilibrium conditions may have been perturbed. Additional iterations in "*while loop*" are then carried out to ensure that both equilibrium and Kuhn-Tucker conditions are satisfied.

The algorithms described in Box 1and Box 2 allow a rapid determination of the structural strains at a through-thickness section of welded plate components once elastic traction stresses along a given weld line have been obtained. The structural strains can then be used for low cycle fatigue evaluation, which will be demonstrated in one of the latter sections.

3.1.2. Pipe section

To obtain structural strain in a pipe section in Sec. 2.2.3, as illustrated in Fig. 5, the numerical procedures are similar to those given in Sec. 3.1.1. Since there exists only one dominant stress component in dealing with a pipe section, the solution process is much simpler. The corresponding numerical algorithm is summarized in Box 3, with its corresponding classical return mapping algorithm being provided in Box 4. In Box 4, it is important to note that for updating equivalent plastic strain using Eq.(20)-(21), $|\sigma_1|$ can be calculated from trial stress and $sign(\sigma_1)$ is typically unknown due to $\sigma_1$is not available prior to plastic strain. However, this problem can be solved by replacing $sign(\sigma_1)$ to $sign(\sigma_1^{tr})$ as shown in:

$$\begin{aligned} |\sigma_1| &= |\sigma_1^{tr}| - E\Delta\bar{\varepsilon}^p \\ sign(\sigma_1) &= sign(\sigma_1^{tr}) \end{aligned} \tag{28}$$

Note that the proof of (28) is provided in Appendix B. By following the numerical algorithms given in Box 3 and Box 4, structural strain can be determined with respect to a pipe cross-section once remote traction stress conditions are prescribed by means of the mesh-insensitive method [1].

Box 3. Overall algorithm for computing structural strain at a pipe section

Set $\varepsilon^{p}_{1,(0)}(y_t)=0, \varepsilon^{p}_{3,(0)}(y_t)=0, \bar{\varepsilon}^{p}_{(0)}(y_t)=0$

while $\left(\left|k_{(i+1)}-k_{(i)}\right|>tol \text{ or } \left|b_{(i+1)}-b_{(i)}\right|>tol \text{ or } \max\left(f^{tr}_{(i+1)}\right)>0\right)$

1. perform "elastic step"

$$\varepsilon_1^{p,tr}(y_t)=\varepsilon^{p}_{1,(i)}(y_t), \varepsilon_3^{p,tr}(y_t)=\varepsilon_3^{p}(y_t), \bar{\varepsilon}^{\,p,tr}(y_t)=\bar{\varepsilon}^{\,p}(y_t)$$

$$Eb_{(i+1)}=\sigma_m+\frac{\int_{-1}^{1}\left(E\varepsilon_1^{p}/\sigma_0\right)l(y')\,dy'}{\pi\left[1-(r/R)^2\right]}$$

$$Ek_{(i+1)}R=\sigma_b+\frac{\int_{-1}^{1}\left(E\varepsilon_1^{p}/\sigma_0\right)l(y')\,y'\,dy'}{(\pi/4)\left[1-(r/R)^4\right]}$$

$$E\varepsilon_{1,(i+1)}(y')=Ek_{(i+1)}Ry'+Eb_{(i+1)}$$

2. calculate trial stress

$$\sigma_1^{tr}(y')=EkRy'+Eb-E\varepsilon_1^{p,tr}(y')$$

$$f^{tr}(\sigma_1^{tr},\bar{\varepsilon}^{\,p})=\left|\sigma_1^{tr}\right|-\sigma_0\left(\frac{E\bar{\varepsilon}^{\,p,tr}}{\alpha\sigma_0}+r^m\right)^{1/m}$$

3. check yield criteria and Kuhn-Tucker complementarity condition

$$f^{tr}(\sigma_1^{tr},\bar{\varepsilon}^{\,p})=\left|\sigma_1^{tr}\right|-\sigma_0\left(\frac{E\bar{\varepsilon}^{\,p,tr}}{\alpha\sigma_0}+r^m\right)^{1/m}$$

if $f^{tr}\le 0$

Elastic step: set $(\bullet)_{(i+1)}=(\bullet)^{tr}$

Else

Plastic step: Proceed with return mapping algorithm (see Box 4)

End if

End while

Box 4 : Return mapping algorithm for pipe section used in Box 3

1.solve $\Delta\tilde{\sigma}^p$:

$$f(\sigma_1,\bar{\varepsilon}^p)=|\sigma_1|-\sigma_0\left(\frac{E\bar{\varepsilon}^p}{\alpha\sigma_0}+r^m\right)^{1/m}=0\Rightarrow$$

$$f(\sigma_1,\bar{\varepsilon}^p)=\left|\sigma_1^{tr}\right|-E\Delta\bar{\varepsilon}^p-\sigma_0\left(\frac{E\bar{\varepsilon}^p}{\alpha\sigma_0}+r^m\right)^{1/m}=0\Rightarrow$$

$$f(\sigma_1,\bar{\varepsilon}^p)=\left|\sigma_1^{tr}\right|-E\Delta\bar{\varepsilon}^p-\sigma_0\left[\frac{E(\bar{\varepsilon}_t^p+\Delta\bar{\varepsilon}^p)}{\alpha\sigma_0}+r^m\right]^{1/m}=0$$

$$f(\sigma_1,\bar{\varepsilon}^p)=\left|\sigma_1^{tr}\right|-E\Delta\bar{\varepsilon}^p-\sigma_0\left[\frac{E(\bar{\varepsilon}^{p,tr}+\Delta\bar{\varepsilon}^p)}{\alpha\sigma_0}+r^m\right]^{1/m}=0$$

solve $\Delta\bar{\varepsilon}^p$ (Newton iteration)

2.update strain and stress

$$\Delta\varepsilon_1^p=\Delta\bar{\varepsilon}^p\times sign(\sigma_1^{tr})$$

$$\varepsilon_1^{p,(i+1)}=\varepsilon_1^{p,(i)}+\Delta\varepsilon_1^p$$

$$\bar{\varepsilon}^p=\bar{\varepsilon}^{p(i)}+\Delta\bar{\varepsilon}^p$$

$$\sigma_1=EkRy'+Eb-E\varepsilon_1^p$$

3.2. FEA based validations

To validate the numerical procedures presented in the last section for calculating structural strain from the governing equations given in Sec. 3.1, commercial FE software ABAQUS [31] is used here for computing structural strain in a plate section modeled as a 2D plane-strain problem, as shown in Fig. 6a. The remote loading condition is prescribed as $\sigma_m = 0.6\sigma_0$ and $\sigma_b = 0.25\sigma_0$. Both stress and structural strain distributions calculated during loading and after unloading are compared in Figs. 6b and 6c, respectively, between FEA solutions and the results obtained using the analytical formulations developed in this study. Note that the material considered here is ASTM A302-B steel and the

corresponding Ramberg-Osgood material parameter is documented in [29]. In the modified Ramberg-Osgood material model, the normalized proportional limit of the material is found to be 0.7, i.e., $r = 0.7\sigma_0$. An applied remote traction stress is at $\sigma_m + \sigma_b = 0.85\sigma_0 > 0.7\,\sigma_0$ so that a certain extent of plastic deformation is expected. It should be emphasized here that σ_0 in Ramberg-Osgood equation is a reference stress and typically greater than the yield strength σ_Y of the material.

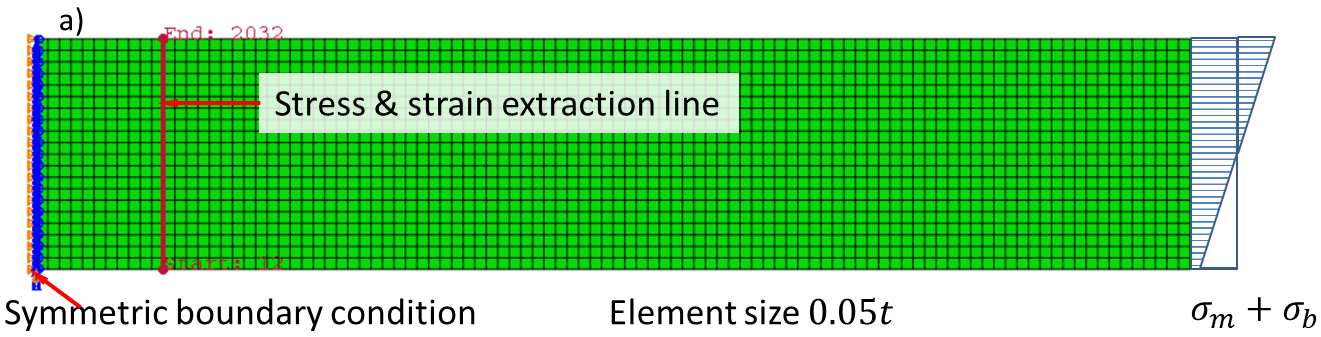

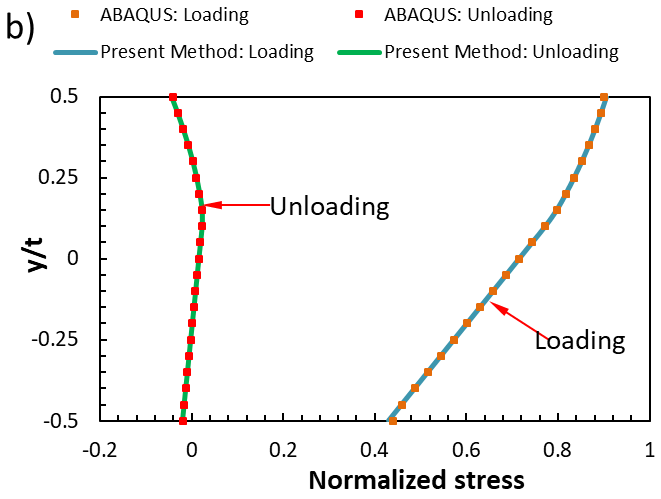

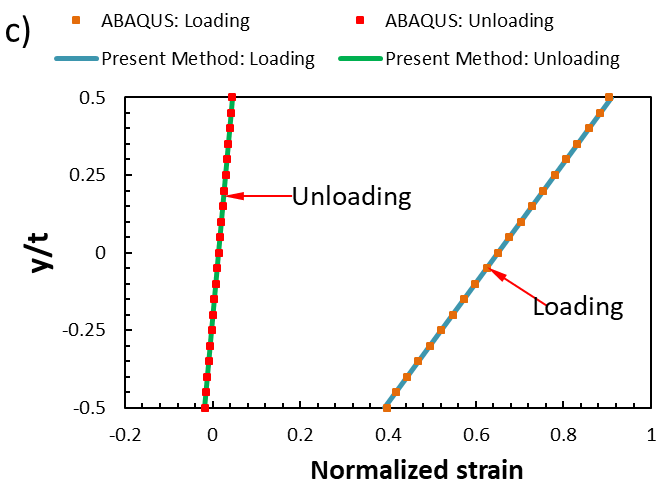

Fig. 6. Comparison of FEA results with the results obtained by the present analytical formulation for a plate section. a) finite element model used b) comparison of stress distributions. c) comparison of structural strains.

The element type used here for performing ABAQUS based FE analysis is 4-node bilinear plane strain elements with hybrid integration scheme for constant pressure, i.e., "CPE4H" which is specifically formulated for large plastic strain problems. As shown in Fig. 6, the analytically formulated structural strain method implemented in the form of numerical algorithms developed in this study show an excellent agreement with the FEA results, validating both the analytical formulations and numerical procedures. The finite element results in terms of total strain in Fig. 6b further validates the appropriateness of the "through thickness linear deformation gradient" assumption since there is no linear strain gradient constraints imposed in obtaining the finite element solutions.

As for structural strain calculations for a pipe section, beam element type "B21" in ABAQUS is used here. Due to the anticipated extent of plastic deformation involved, a total of 56 additional integration points beyond the default value of 25 were introduced for a better resolution of beam section plastic deformation behavior, as illustrated in Fig. 7a. The material considered in the pipe section is identical to the one used in the plate section problem shown in Fig. 6. The results are compared in Fig. 7b in terms of stresses and Fig. 7c in terms of strains with the results obtained through the analytical formulation developed in this study. Again, an excellent agreement between the two independent solutions can be seen in both Figs. 7b and 7c, validating the present approach for applications in pipe sections.

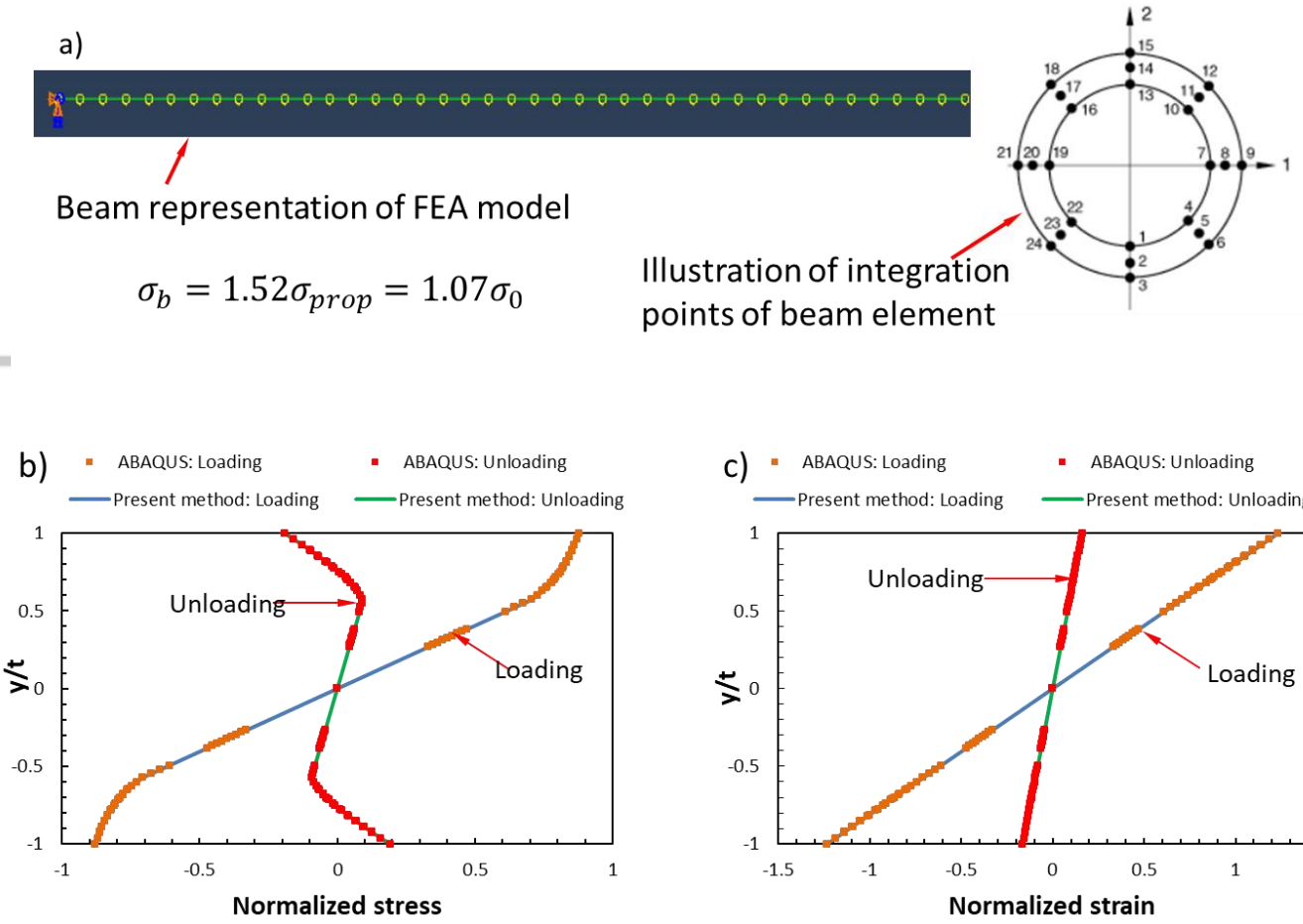

Fig. 7 Comparison of FE results with the results obtained using the analytical formulations developed in this paper for a pipe section: a) beam element model representing a pipe section; b) comparison of stress distributions. c) comparison of structural strains.

3.3. Application in fatigue test data correlation

Three independent sets of fatigue test data of welded components with fatigue lives spanning both high-cycle and low-cycle regimes are considered here. The first set represents filleted welded plate-gusset specimen tests performed by The Welding Institute (TWI) [33], the second set contain girth-welded pipes sponsored by Welding Research Council (WRC) [18], and the third involves fatigue tests of girth welded pipe to nozzle fitting connections by Paulin Research Group

(PRG) [34]. Materials used in these tests involve high strength low alloy steels, low carbon steels, and 304 stainless steel. Details can be found in their reports. It should also be noted that the gusset-on-plate specimen tests by TWI [33] were carried out under load-controlled conditions while the tests by PRG [34] and WRC [18] were performed under displacement-controlled conditions. Nominal strain measurements are available for tests performed by PRG and WRC while only nominal stress range are available for tests performed by TWI. All three sets of fatigue test results are plotted in Fig. 8 in terms of nominal strain range versus cycle to failure. Note that due to the lack of measured strains in TWI's tests, the nominal strains are calculated based on nominal stress ranges provided by the nominal stress ranges divided by steel Young's modulus.

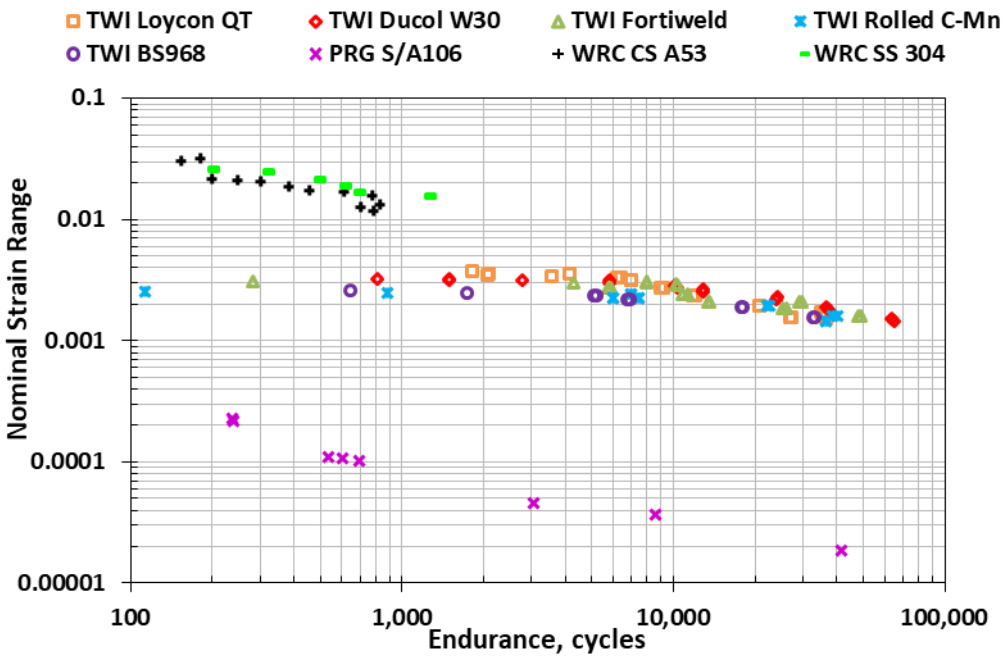

Fig. 8. Correlation of fatigue test data using measured strain (PRG and WRC) and nominal strain (TWI)

Due to differences in measurement locations as well as calculated strains based on nominal stresses, the three sets of test data follow three separate trend lines, as expected. Furthermore, test data obtained under load-controlled conditions by

TWI exhibit a "flattened off" region in low-cycle fatigue regime, which is a common feature when a stress based parameter is used.

In contrast, once all these test data are plotted in terms of structural strain parameter $\Delta\epsilon_s$ calculated from the analytical formulation given in Sec. 2, a single narrow and approximately straight band can be seen in Fig. 9, covering data from very low cycle fatigue regime (a few hundreds of cycles to failure) to a regime corresponding to high cycle fatigue (at 10^5 cycles to failure). This suggests that the structural strain parameter serves as a good fatigue parameter for fatigue characterization in both low cycle and high cycle regimes. The effectiveness of the structural strain parameter in correlating both low and high cycle fatigue data further substantiates the fact that fatigue damage is strain-controlled phenomenon, rather than stress-controlled. Instead of using a notch strain based parameter widely discussed in literature [6,12,13], the present study introduces a cross-section based structural strain definition, which can be directly implemented for applications in complex structures and loading conditions. Further discussions, additional validations, as well as proposed implementation in codified procedures [35] will be presented in an ensuing paper [36].

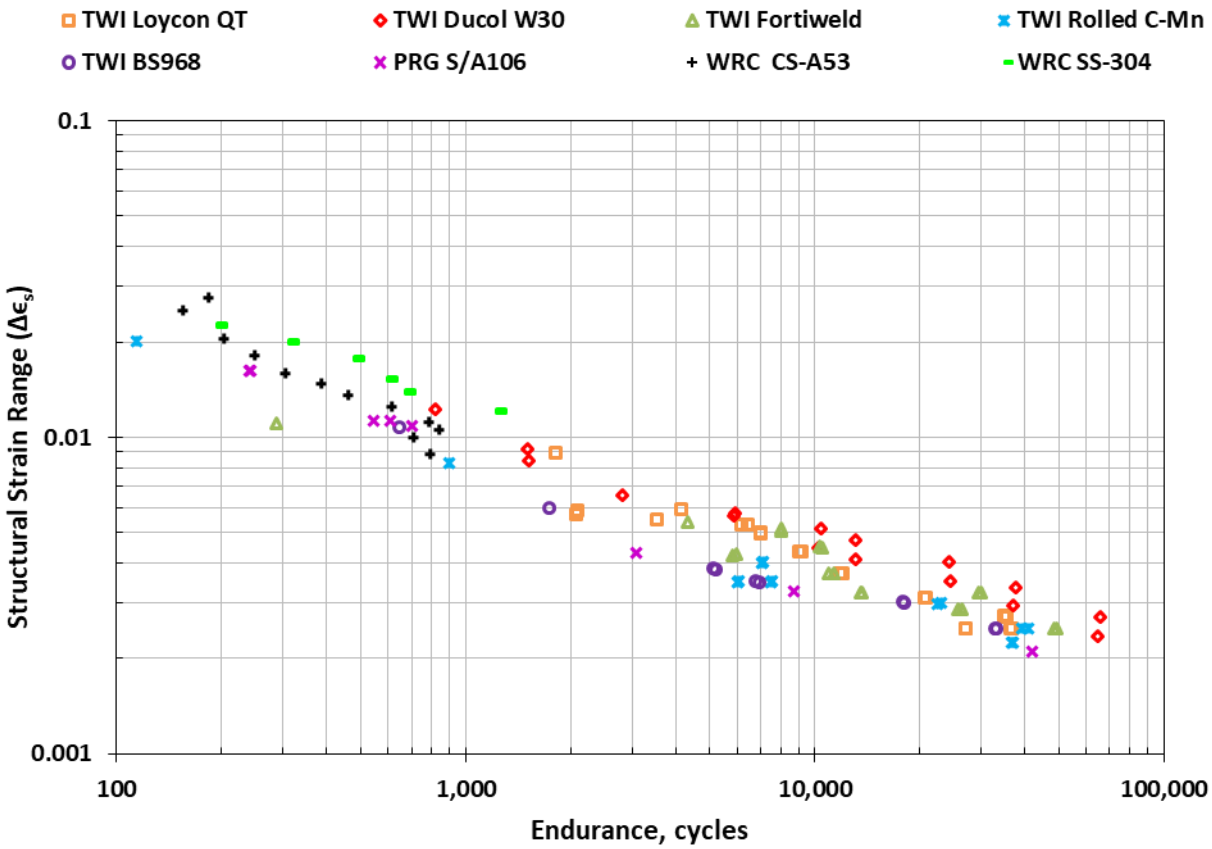

Fig. 9 Correlation of fatigue test data from PRG, TWI, and WRC using structural strain range calculated using the formulations developed in this study

4. Discussions

4.1. Plane stress versus plane strain conditions

Dong et al. [21] first introduced the "structural strain" method for evaluating low-cycle fatigue behaviors of welded components. For simplicity, they assumed plane stress conditions in order to obtain closed form solutions of structural strain as a correction to elastically calculated traction structural stresses. As a result, the applicability of their structural strain solutions is restricted to small scale yielding conditions. For most structural applications, plane-strain conditions

should be more appropriate when a plate cross-section is considered as discussed in this paper. With the new developments presented in this paper, plane-strain conditions can now be treated with ease. Then, it should be informative to examine the applicability of the two conditions in structural strain calculations.

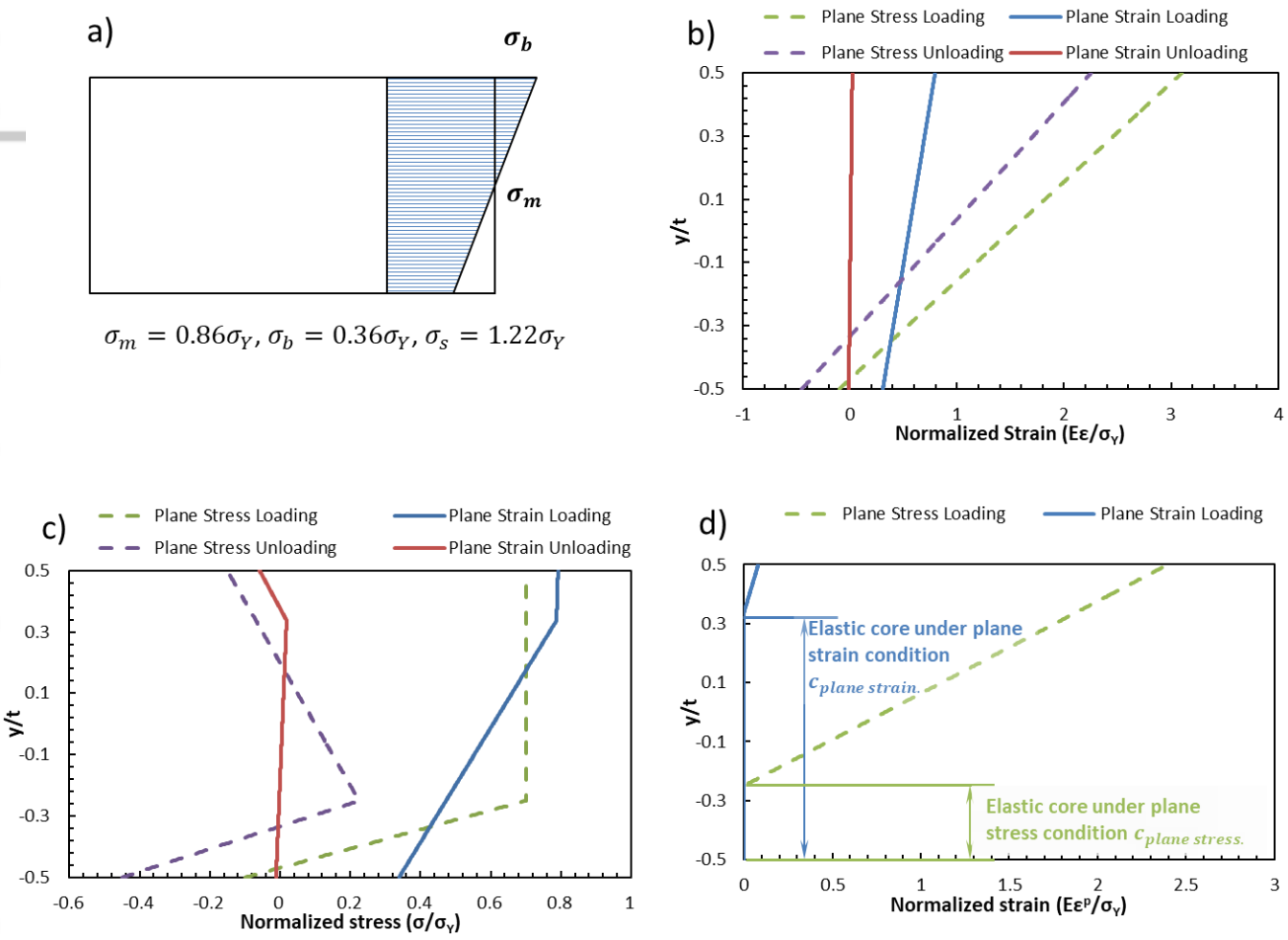

Fig. 10. Comparison of section behavior under plain stress and plain strain condition: a) Load definition b) comparison of total strain distribution c) comparison of normal stress distribution d) comparison of plastic strain distribution

Consider a plate through-thickness section subjected to remote membrane and bending stresses of $\sigma_m = 0.86\sigma_Y$ and $\sigma_b = 0.36\sigma_Y$, respectively, as shown in Fig. 10a. At first, elastic perfectly plastic material model is considered. Fig. 10b shows the comparison of the structural strain results between the two cases, both during loading and after unloading. As can be

clearly seen, the calculated structural strains under plane-stress conditions is about three times that under plane-strain conditions. Such a large difference in structural strain results can be readily explained by examining Fig. 10c in terms of differences in resulting stress distributions and Fig. 10d in terms of elastic core sizes. The extent of plastic deformation under plane stress conditions is so large, with an elastic core be reduced to only about 20% of the plate thickness or 0.2t, while under plane strain conditions, the corresponding elastic core size still remains at $0.8t$, which is four times bigger than that under plane stress conditions. The results in Fig. 10 strongly suggest that that plane strain conditions should be used in general for computing structural strains for performing low cycle fatigue evaluation of plate structures.

4.2. Effect of material strain hardening

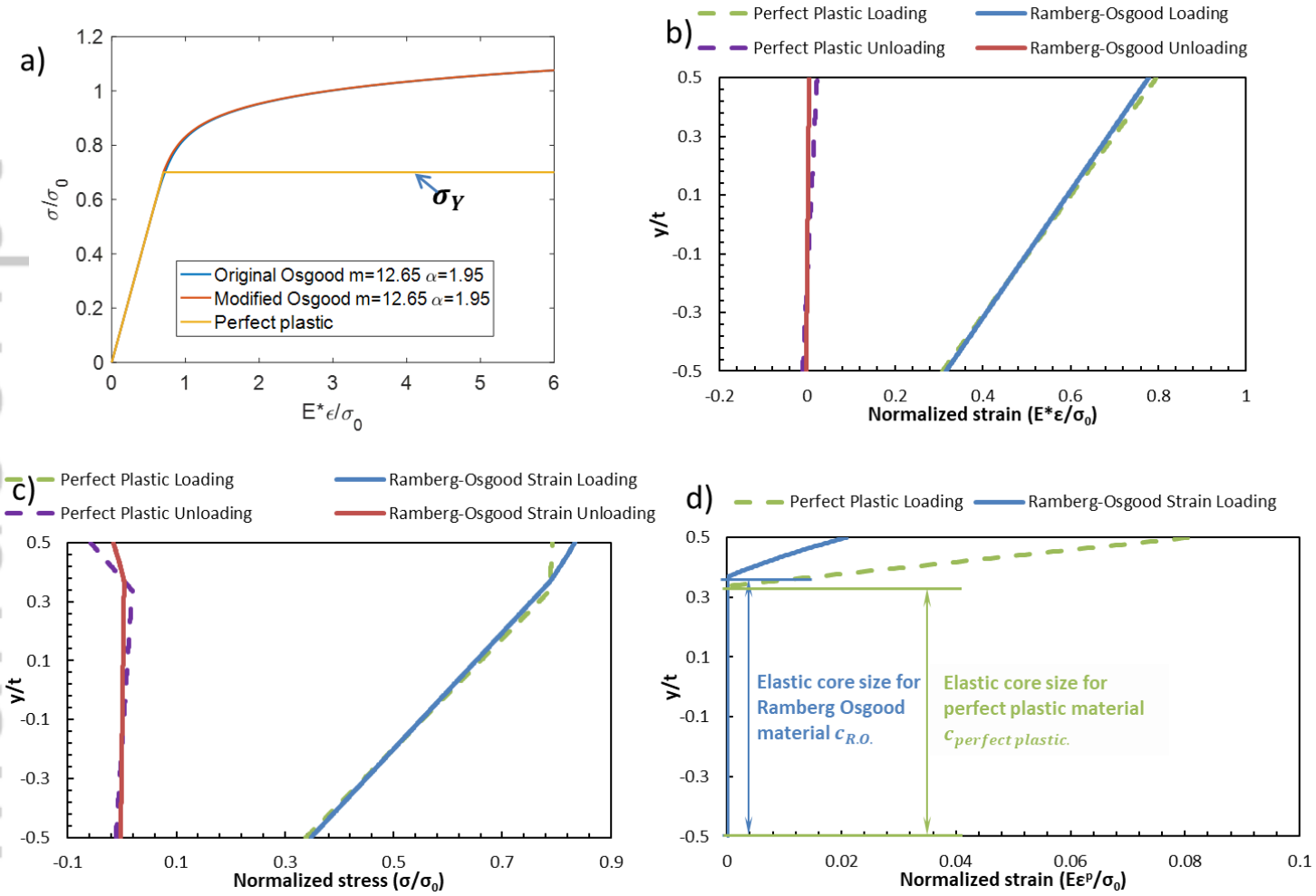

Fig. 11 Comparison of section behavior with and without strain hardening consideration: a) stress-strain curve comparison b) comparison of structural strain (total strain) distribution c) comparison of normal stress distribution d) comparison of plastic strain distribution

Consider the same plate section examined in Fig. 10, subjected to remote loading conditions corresponding to $\sigma_m = 0.6\sigma_0$ and $\sigma_b = 0.25\sigma_0$, in which σ_0 is the reference stress. And Ramberg-Osgood parameters used here are $\alpha = 1.95, m = 12.65$, and $\sigma_{prop} = 0.7\sigma_0$. For the case with elastic perfectly plastic model, yield stress of the material is set as $\sigma_Y = 0.7\sigma_0$. Plane strain conditions are considered in both cases.

The structural strain results for the two cases are compared in Fig. 11b, showing rather insignificant differences both at loading and after unloading stage. The local stress results show a more noticeable difference between the two cases in Fig. 11c in a region corresponding $y > 0.3t$ in which both cases experience plastic deformation. Fig. 11d shows that the peak local plastic strain value for the case of elastic perfectly plastic material is about 4 times greater than that for the case of Ramberg-Osgood material while the difference in elastic core size between the two is only about 4%, i.e., being negligible. Both the structural strain results in Fig. 11b and elastic core size results shown in Fig. 11d seem to confirm the postulation by Dong et al. [21] that the structural strain is dominated by elastic core size. The results also suggest that if Ramberg-Osgood material parameters are not available for a material of interest, the use of elastic perfectly plastic model can still yield a reasonable estimation of structural strain for low cycle fatigue evaluation purpose.

5. Conclusions

In this paper an analytically formulated structural strain method is presented for fatigue evaluation of welded components:

- A modified Ramberg-Osgood power-law hardening model is developed to incorporating nonlinear material hardening behaviors. The modified Ramberg-Osgood power-law hardening model enables a consistent partitioning of elastic and plastic strain increments during both loading and unloading, which enables people to determining both structural strain and elastic core size numerically.
- The new structural strain method is cast in two forms for facilitating fatigue evaluation of two major forms welded structures used in industry: one is for structural strain determination with respect to a through-thickness section in plate structures; the other for structural strain determination with respect to pipe cross-section in piping systems.
- The structural strain is defined as the linearly distributed total strain (linear deformation gradient) on the cross-section, consistent with the "plane sections remain plane" assumption in the context of structural mechanics.

- A set of robust numerical procedures are presented for solving the analytically formulated structural strain expressions.
- The structural strain based fatigue parameter proposed has been shown effective in correlating some well-known low cycle and high cycle fatigue test data from three independent laboratories, ranging from mild steel to high strength steel weldments, from gusset-to-plate welded plate connections to pipe girth welds.

With the new developments presented in this paper, the structural strain method can be used as a post-processing procedure applied to linear elastic traction structural stresses obtained at a given plate or pipe cross-section by the mesh-insensitive structural stress method adopted by ASME Div 2 since 2007, which can be used for complex structures and loading conditions. The resulting master E-N curve serves as a natural extension of the master S-N curve which is dominated by high cycle fatigue test data into low cycle regime, as shown in Fig. 9, which will be further substantiated by an ensuring paper by the same authors [36].

6. Acknowledgement

The authors gratefully acknowledge the support of this work in part by ONR Grant No. N00014-10-1-0479 at UNO and the National Research Foundation of Korea (NRF) Gant funded by the Korea government (MEST) through GCRC-SOP at University of Michigan under Project 2-1: Reliability and Strength Assessment of Core Parts and Material System. P. Dong also acknowledges partial financial support made possible by Traction Power National Key Laboratory Open Competition Grant (No. TPL 1605).

Reference

[1] Dong, P. (2001). A structural stress definition and numerical implementation for fatigue analysis of welded joints. International Journal of Fatigue, 23(10), 865-876.

[2] Code of practice for fatigue design and assessment of steel structures. BS7608, British Standards Institution, 1993.

[3] Design of steel structures—Part 1-1. ENV 1993-1-1. Eurcode 3, European Committee for Standardization, Brussels, 1992.

[4] Hobbacher A. Fatigue design of welded joints and components: Recommendations of IIW Joint Working Group XIII–XV. Abington, Cambridge: Abington Publishing, 1996.

[5] Hobbacher A. Basic philosophy of the new IIW recommendations on fatigue design of welded joints and components. Welding in the World 1997;39(5):272–8

[6] Radaj D. Review of fatigue strength assessment of non-welded and welded structures based on local parameters. International Journal of Fatigue 1996;18(3):153–70.

[7] Lawrence FV, Mattos RJ, Higashida Y, Burk JD. Estimating the fatigue crack initiation life of welds. ASTM STP 1978;648:134–58.

[8] Dong, P., Hong, J. K., & De Jesus, A. M. (2007). Analysis of recent fatigue data using the structural stress procedure in ASME Div 2 rewrite. Journal of Pressure Vessel Technology, 129(3), 355-362.

[9] AASHTO. LRFD 2004. AASTO LRFD bridge design specifications, 3rd Ed., Washington, D.C.

[10] Zhang, G., and B. Richter. "A new approach to the numerical fatigue‐life prediction of spot‐welded structures." Fatigue & Fracture of Engineering Materials & Structures 23.6 (2000): 499-508.

[11] ZHANG, GENBAO, Martin EIBL, and Sumanjit SINGH. "Methods of predicting the fatigue lives of laser-beam welded lap welds subjected to shear stresses." Welding and cutting 2 (2002): 96-103.

[12] Morgenstern, C., Sonsino, C. M., Hobbacher, A., & Sorbo, F. (2006). Fatigue design of aluminium welded joints by the local stress concept with the fictitious notch radius of rf= 1 mm. International journal of fatigue, 28(8), 881-890.

[13] Schmidt, H., Baumgartner, J., & Melz, T. (2015). Fatigue assessment of joints using the local stress field. Materialwissenschaft und Werkstofftechnik, 46(2), 145-155.

[14] Dong, P., Hong, J. K., & Cao, Z. (2003). Stresses and stress intensities at notches: 'anomalous crack growth' revisited. International journal of fatigue, 25(9-11), 811-825.

[15] Mei, J., & Dong, P. (2017). An equivalent stress parameter for multi-axial fatigue evaluation of welded components including non-proportional loading effects. International Journal of Fatigue, 101, 297-311.

[16] Dong, P., Cao, Z., & Hong, J. K. (2006, January). Low-cycle fatigue evaluation using the weld master SN curve. In ASME 2006 Pressure Vessels and Piping/ICPVT-11 Conference (pp. 237-246). American Society of Mechanical Engineers.

[17] Markl, A. R. C. "Fatigue tests of piping components." Trans. ASME 74 (1952): 287-303.

[18] Scavuzzo, R.J., Srivatsan, T.S., and Lam, P.C., "Fatigue of Butt-Welded Pipe," Report 1 in Fatigue of Butt-Welded Pipe and Effect of Testing Methods, Welding Research Council Bulletin 433, July 1998.

[19] Dong, P., & Yang, X. (2010, January). A Master SN Curve Representation of Subsea Umbilical Tube Weld Fatigue Data. In ASME 2010 29th International Conference on Ocean, Offshore and Arctic Engineering (pp. 177-184). American Society of Mechanical Engineers.

[20] Gas Transmission and Distribution Piping Systems, ASME B31.8-2003, American Society of Mechanical Engineers, 2003

[21] Dong, P., Pei, X., Xing, S., & Kim, M. H. (2014). A structural strain method for low-cycle fatigue evaluation of welded components. International Journal of Pressure Vessels and Piping, 119, 39-51.

[22] Pei, X., Wang, W., & Dong, P. (2017, July). An Analytical-Based Structural Strain Method for Low Cycle Fatigue Evaluation of Girth-Welded Pipes. In ASME 2017 Pressure Vessels and Piping Conference (pp. V03BT03A015-V03BT03A015). American Society of Mechanical Engineers.

[23] Dong, P., Pei, X., & Xing, S. (2014, June). A Structural Strain Method for Fatigue Evaluation of Welded Components. In ASME 2014 33rd International Conference on Ocean, Offshore and Arctic Engineering (pp. V005T03A037-V005T03A037). American Society of Mechanical Engineers.

[24] American Society of Mechanical Engineers, 1997, ASME Boiler and Pressure Vessel code, Section 3, Rules for Construction of Nuclear Power Plant Components, NB, Class 1 Components and Section VIII, Rules for Construction of Pressure Vessels, Division 2-Alternate Rules.

[25] Ramberg, Walter, and William R. Osgood. "Description of stress-strain curves by three parameters." (1943).

[26] Basan, Robert, et al. "Study on Ramberg-Osgood and Chaboche models for 42CrMo4 steel and some approximations." Journal of Constructional Steel Research 136 (2017): 65-74.
[27] Ning Liu, and Ann E. Jeffers. "Adaptive isogeometric analysis in structural frames using a layer-based discretization to model spread of plasticity." Computers & Structures 196 (2018): 1-11.
[28] Zappalorto, M., and L. Maragoni. "Nonlinear mode III crack stress fields for materials obeying a modified Ramberg‐Osgood law." Fatigue & Fracture of Engineering Materials & Structures 41.3 (2018): 708-714.
[29] Qian, Lingxi. "Principle of complementary energy",Science in China Series A 1.2 (1950): 449- 456.
[30] Simo, J. C., & Hughes, T. J. (2006). Computational inelasticity (Vol. 7). Springer Science & Business Media.
[31] Hibbit Karlson, Sorensen Inc, ABAQUS Version 6.12, 2003.
[32] James, L. A. "Ramberg-Osgood Strain-Hardening Characterization of an ASTM A302-B Steel." Journal of pressure vessel technology 117.4 (1995): 341-345.
[33] Harrison, J. D. "Fatigue Performance of Welded High Strength Steels, A compendium of reports from sponsored research programme." The Welding Institute, Abington Hall, Arbinton, Cambridge CBI 6AL, England (1974).
[34] Hinnant, Chris, and Tony Paulin. "Experimental Evaluation of the Markl Fatigue Methods and ASME Piping Stress Intensification Factors." ASME 2008 Pressure Vessels and Piping Conference. American Society of Mechanical Engineers, 2008.
[35] Osage, D. A., Dong, P., & Spring, D. (2018). Fatigue assessment of welded joints in API 579-1/ASME FFS-1 2016-existing methods and new developments. Procedia Engineering, 213, 497-538.
[36] Pei, X and Dong, P, Application of structural strain method for fatigue evaluation of welded components of different materials (to be submitted)

Appendix A: Idea of Modified Ramberg-Osgood Equation

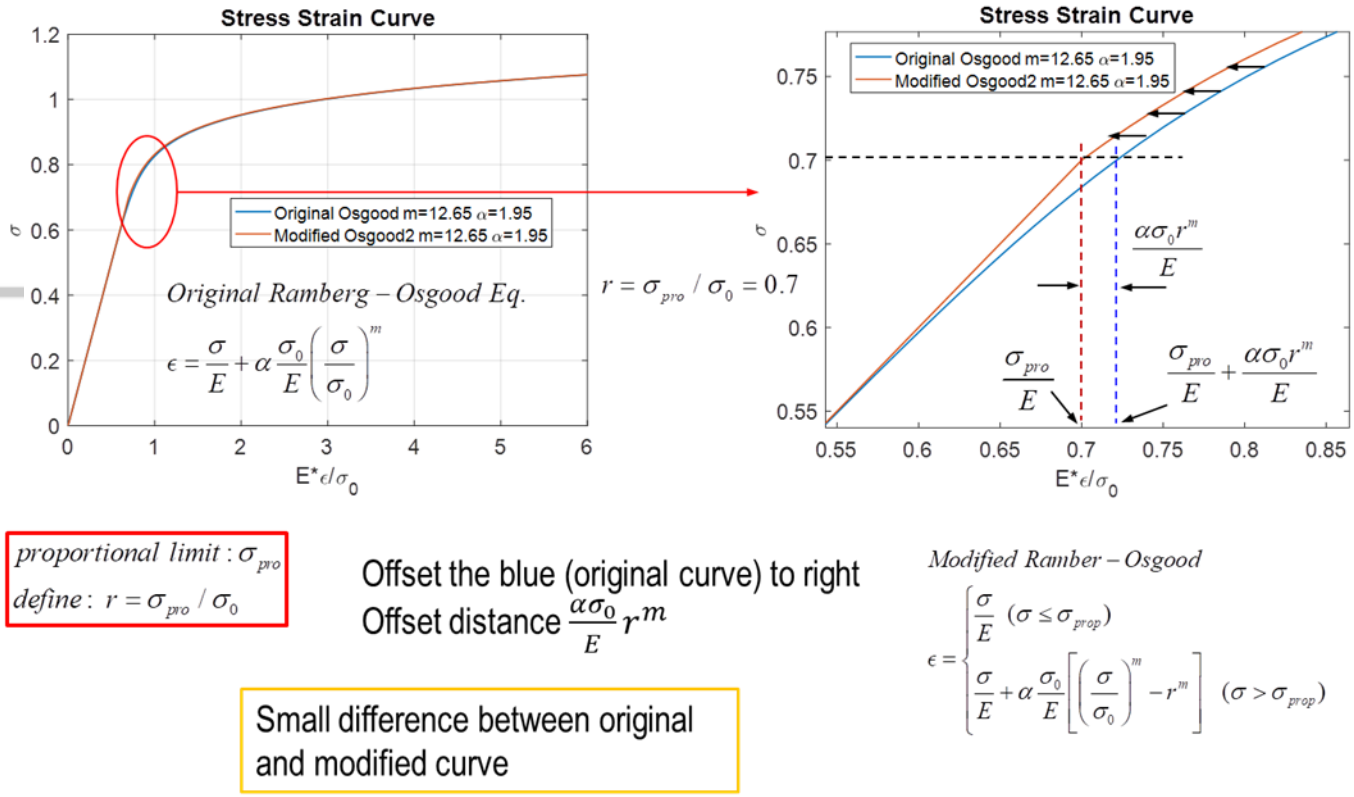

Fig. A1Illustration of idea of modified Ramberg-Osgood equation

Fig. A1 demonstrates the idea of modified Ramberg-Osgood equation: when $\sigma = \sigma_{pro}$, according to the original Ramberg-Osgood equation, the total strain is $\varepsilon = \sigma_{pro}/E + \alpha\sigma_0 r^m/E$ (here $r = \sigma_{pro}/\sigma_0$). However, by definition, below material proportional limit σ_{pro}, there should be only elastic strain, i.e. $\varepsilon = \sigma_{pro}/E$. In the modified Ramberg-Osgood equation, the total strain is offset by $\alpha\sigma_0 r^m/E$, when the stress is beyond material proportional limit. According to modified Ramberg-Osgood equation, there is no nonlinear term when applied stress is less then proportional limit σ_{pro}.

Appendix B: Proof of Eq. (27)

Here a time step from t to $t+\Delta t$ is considered. And in what follows, all quantities are taken to be those at the end of a time step, i.e., at $t+\Delta t$, unless specifically stated. So the stress at $t+\Delta t$ is just noted as $\boldsymbol{\sigma}$ rather than $\boldsymbol{\sigma}_{t+\Delta t}$, for simplicity. The quantities at beginning of a time step is described using a subscript t, for example, stress at beginning of the time step is noted as $\boldsymbol{\sigma}_t$.

As given in Eq. (11) and (12), stress strain relationship of small strain theory is as follows

$$\begin{aligned}\boldsymbol{\sigma} &= 2G\boldsymbol{\varepsilon}^e + \lambda Tr\left(\boldsymbol{\varepsilon}^e\right)\boldsymbol{I} \\ \lambda &= \frac{E\nu}{(1+\nu)(1-2\nu)}\end{aligned} \tag{App.1}$$

The strain decomposition in the time step is given by:

$$\boldsymbol{\varepsilon}^{\boldsymbol{e}} = \boldsymbol{\varepsilon}_{\boldsymbol{t}}^{\boldsymbol{e}} + \boldsymbol{\Delta\varepsilon}^{\boldsymbol{e}} = \boldsymbol{\varepsilon}_{\boldsymbol{t}}^{\boldsymbol{e}} + \boldsymbol{\Delta\varepsilon} - \boldsymbol{\Delta\varepsilon}^{\boldsymbol{p}} \tag{App.2}$$

From (App.1) and (App.2), we have:

$$\begin{aligned}\boldsymbol{\sigma} &= 2G\left(\boldsymbol{\varepsilon}^e + \Delta\boldsymbol{\varepsilon} - \Delta\boldsymbol{\varepsilon}^p\right) + \lambda Tr\left(\boldsymbol{\varepsilon}^e + \Delta\boldsymbol{\varepsilon} - \Delta\boldsymbol{\varepsilon}^p\right)\boldsymbol{I} \\ \boldsymbol{\sigma} &= 2G\left(\boldsymbol{\varepsilon}^e + \Delta\boldsymbol{\varepsilon}\right) + \lambda Tr\left(\boldsymbol{\varepsilon}^e + \Delta\boldsymbol{\varepsilon}\right)\boldsymbol{I} - 2G\Delta\boldsymbol{\varepsilon}^p\end{aligned} \tag{App.3}$$

Here in Eq.(App.3), incompressibility for plasticity condition is used, which is

$$Tr\left(\Delta\boldsymbol{\varepsilon}^p\right) = \Delta\varepsilon_1^p + \Delta\varepsilon_2^p + \Delta\varepsilon_3^p = 0 \tag{App.4}$$

Define trial stress $\boldsymbol{\sigma}^{tr}$ as:

$$\boldsymbol{\sigma}^{tr} = 2G\left(\boldsymbol{\varepsilon}^e + \Delta\boldsymbol{\varepsilon}\right) + \lambda Tr\left(\boldsymbol{\varepsilon}^e + \Delta\boldsymbol{\varepsilon}\right)\boldsymbol{I} \tag{App.5}$$

Also due to incompressibility condition,

$$\begin{aligned} Tr(\boldsymbol{\sigma}) &= Tr\left[2G\left(\boldsymbol{\varepsilon}^e + \Delta\boldsymbol{\varepsilon}\right) + \lambda Tr\left(\boldsymbol{\varepsilon}^e + \Delta\boldsymbol{\varepsilon}\right)\boldsymbol{I} - 2G\Delta\boldsymbol{\varepsilon}^p\right] \\ &= Tr\left[2G\left(\boldsymbol{\varepsilon}^e + \Delta\boldsymbol{\varepsilon}\right) + \lambda Tr\left(\boldsymbol{\varepsilon}^e + \Delta\boldsymbol{\varepsilon}\right)\boldsymbol{I}\right] - 2GTr\left(\Delta\boldsymbol{\varepsilon}^p\right) \\ &= Tr\left[2G\left(\boldsymbol{\varepsilon}^e + \Delta\boldsymbol{\varepsilon}\right) + \lambda Tr\left(\boldsymbol{\varepsilon}^e + \Delta\boldsymbol{\varepsilon}\right)\boldsymbol{I}\right] = Tr\left(\boldsymbol{\sigma}^{tr}\right) \end{aligned} \quad \text{(App.6)}$$

From (App.3) and (App.5):

$$\boldsymbol{\sigma} = \boldsymbol{\sigma}^{tr} - 2G\Delta\boldsymbol{\varepsilon}^p \quad \text{(App.7)}$$

And as already given by Eq. (16) and Eq. (25), for von-Mises yield criteria, $\Delta\boldsymbol{\varepsilon}^p$ is given by:

$$\Delta\boldsymbol{\varepsilon}^p = \frac{3}{2}\Delta\bar{\varepsilon}^p\frac{\boldsymbol{\sigma}'}{\sigma_e} \quad \text{(App.8)}$$

Same as before, σ_e is the von-Mises and $\boldsymbol{\sigma}'$ is deviatoric stress given by:

$$\boldsymbol{\sigma}' = \boldsymbol{\sigma} - \frac{1}{3}Tr(\boldsymbol{\sigma})\boldsymbol{I} \quad \text{(App.9)}$$

Here $\boldsymbol{I}$is 2nd order isotropic tensor (kronecker delta). Combine (App.7) and (App.8), we have

$$\begin{aligned} \boldsymbol{\sigma}^{tr} - 2G\Delta\bar{\varepsilon}^p\frac{3}{2}\frac{\boldsymbol{\sigma}'}{\sigma_e} &= \boldsymbol{\sigma} = \boldsymbol{\sigma}' + \frac{1}{3}Tr(\boldsymbol{\sigma})\boldsymbol{I} \\ \boldsymbol{\sigma}^{tr} - \frac{1}{3}Tr(\boldsymbol{\sigma})\boldsymbol{I} &= \boldsymbol{\sigma}' + 3G\Delta\bar{\varepsilon}^p\frac{\boldsymbol{\sigma}'}{\sigma_e} \end{aligned} \quad \text{(App.10)}$$

Bear (App.6) in mind, (App.10) can be rewrite as:

$$\boldsymbol{\sigma}^{tr} - \frac{1}{3} Tr\left(\boldsymbol{\sigma}^{tr}\right) \boldsymbol{I} = \boldsymbol{\sigma}' + 3G\Delta\bar{\varepsilon}^{p} \frac{\boldsymbol{\sigma}'}{\sigma_e}$$
$$\boldsymbol{\sigma}^{tr'} = \left(1 + 3G\frac{\Delta\bar{\varepsilon}^{p}}{\sigma_e}\right)\boldsymbol{\sigma}' \qquad \text{(App.11)}$$

Here $\boldsymbol{\sigma}^{\boldsymbol{tr'}}$ is deviatoric trial stress, and from (App.11)

$$\frac{3}{2}\boldsymbol{\sigma}^{\boldsymbol{tr'}} : \boldsymbol{\sigma}^{\boldsymbol{tr'}} = \left(1 + 3G\frac{\Delta\bar{\varepsilon}^{p}}{\sigma_e}\right)^2 \frac{3}{2}\boldsymbol{\sigma}' : \boldsymbol{\sigma}' \qquad \text{(App.12)}$$

Notice that by the definition of von-Mises, one can write

$$\sigma_e^2 = \frac{3}{2}\boldsymbol{\sigma}' : \boldsymbol{\sigma}' \qquad \text{(App.13)}$$

Leading to

$$\left(\sigma_e^{tr}\right)^2 = \left(1 + 3G\frac{\Delta\bar{\varepsilon}^{p}}{\sigma_e}\right)^2 \sigma_e^2 \qquad \text{(App.14)}$$

And finally reachs to Eq.(27)

$$\sigma_e^{tr} = \left(1 + 3G\frac{\Delta\bar{\varepsilon}^{p}}{\sigma_e}\right)\sigma_e$$
$$\sigma_e = \sigma_e^{tr} - 3G\Delta\bar{\varepsilon}^{p} \qquad \text{(App.15)}$$

Appendix C: Proof of Eq. (28)

According to elastic stress-strain relationship and definition of trial stress:

$$\sigma_1 = E\left(\varepsilon_1 - \varepsilon_1^p\right) = E\left(\varepsilon_1 - \varepsilon_{1,t}^p\right) + E\left(\varepsilon_{1,t}^p - \varepsilon_1^p\right)$$
$$\sigma_1 = \sigma_1^{tr} - E\Delta\gamma \times sign(\sigma_1) \tag{App.16}$$

Notice that

$$\sigma_1 = \left|\sigma_1\right| sign(\sigma_1) \tag{App.17}$$

Eq.(App.16) can be rewrited as:

$$\left|\sigma_1\right| sign(\sigma_1) = \left|\sigma_1^{tr}\right| sign\left(\sigma_1^{tr}\right) - E\Delta\gamma \times sign(\sigma_1)$$
$$\left[\left|\sigma_1\right| + E\Delta\gamma\right] sign(\sigma_1) = \left|\sigma_{n+1}^{trial}\right| sign\left(\sigma_{n+1}^{trial}\right) \tag{App.18}$$

Due to $\Delta\gamma$ is greater or equal to zero by definition of plastic multiplier,

$$\left[\left|\sigma_1\right| + E\Delta\gamma\right] \geq 0$$
$$\left|\sigma_{n+1}^{trial}\right| \geq 0 \tag{App.19}$$

Combining (App.18) and (App.19), we have:

$$sign(\sigma_1) = sign(\sigma_1^{tr}) \tag{App.20}$$